Monthly Notices
of the
ROYAL ASTRONOMICAL SOCIETY

MNRAS **472,** 808–827 (2017)
Advance Access publication 2017 August 18

doi:10.1093/mnras/stx2096

The VMC survey – XXV. The 3D structure of the Small Magellanic Cloud from Classical Cepheids

Vincenzo Ripepi,[1]★ Maria-Rosa L. Cioni,[2,3]★ Maria Ida Moretti,[1] Marcella Marconi,[1]★ Kenji Bekki,[4] Gisella Clementini,[5] Richard de Grijs,[6,7] Jim Emerson,[8] Martin A. T. Groenewegen,[9] Valentin D. Ivanov,[10,11] Roberto Molinaro,[1] Tatiana Muraveva,[5] Joana M. Oliveira,[14] Andrés E. Piatti,[12,13] Smitha Subramanian[6] and Jacco Th. van Loon[14]

[1]*INAF-Osservatorio Astronomico di Capodimonte, via Moiariello 16, I-80131 Naples, Italy*
[2]*Leibniz-Institüt fü Astrophysik Potsdam, An der Sternwarte 16, D-14482 Potsdam, Germany*
[3]*Physics Astronomy and Mathematics, University of Hertfordshire, College Lane, Hatfield AL10 9AB, UK*
[4]*ICRAR M468, The University of Western Australia, 35 Stirling Hwy, Crawley, Western Australia 6009, Australia*
[5]*INAF-Osservatorio Astronomico di Bologna, Via Gobetti 93/3, I-40129 Bologna, Italy*
[6]*Department of Astronomy, Kavli Institute for Astronomy and Astrophysics, Peking University, Yi He Yuan Lu 5, Hai Dian District, Beijing 100871, China*
[7]*International Space Science Institute–Beijing, 1 Nanertiao, Zhongguancun, Hai Dian District, Beijing 100190, China*
[8]*Astronomy Unit, School of Physics and Astronomy, Queen Mary University of London, Mile End Road, London E1 4NS, UK*
[9]*IKoninklijke Sterrenwacht van België, Ringlaan 3, B-1180 Brussels, Belgium*
[10]*European Southern Observatory, Ave. Alonso de Cordova 3107, Vitacura, Casilla 19001, Santiago, Chile*
[11]*European Southern Observatory, Karl-Schwarzschild-Str 2, D-85748 Garching bei München, Germany*
[12]*Observatorio Astronómico, Universidad Nacional de Córdoba, Laprida 854, 5000 Córdoba, Argentina*
[13]*Consejo Nacional de Investigaciones Científicas y Técnicas, Av. Rivadavia 1917, C1033AAJ Buenos Aires, Argentina*
[14]*Lennard-Jones Laboratories, Keele University, Keele, Newcastle-under-Lyme, Staffordshire ST5 5BG, UK*

Accepted 2017 August 10. Received 2017 August 9; in original form 2017 June 16

ABSTRACT

The VISTA near-infrared YJK_s survey of the Magellanic System (VMC) is collecting deep K_s-band time-series photometry of pulsating stars hosted by the two Magellanic Clouds and their connecting bridge. Here, we present Y, J, K_s light curves for a sample of 717 Small Magellanic Cloud (SMC) Classical Cepheids (CCs). These data, complemented with our previous results and V magnitude from literature, allowed us to construct a variety of period–luminosity and period–Wesenheit relationships, valid for Fundamental, First and Second Overtone pulsators. These relations provide accurate individual distances to CCs in the SMC over an area of more than 40 deg^2. Adopting literature relations, we estimated ages and metallicities for the majority of the investigated pulsators, finding that (i) the age distribution is bimodal, with two peaks at 120 ± 10 and 220 ± 10 Myr; (i) the more metal-rich CCs appear to be located closer to the centre of the galaxy. Our results show that the three-dimensional distribution of the CCs in the SMC is not planar but heavily elongated for more than 25–30 kpc approximately in the east/north-east towards south-west direction. The young and old CCs in the SMC show a different geometric distribution. Our data support the current theoretical scenario predicting a close encounter or a direct collision between the Clouds some 200 Myr ago and confirm the presence of a Counter-Bridge predicted by some models. The high-precision three-dimensional distribution of young stars presented in this paper provides a new test bed for future models exploring the formation and evolution of the Magellanic System.

Key words: stars: oscillations – stars: variables: Cepheids – stars: variables: RR Lyrae – Magellanic Clouds – galaxies: structure.

★ E-mail: ripepi@oacn.inaf.it (VR); mcioni@aip.de (M-RLC); marconi@na.astro.it (MM)

1 INTRODUCTION

The Large Magellanic Cloud (LMC) and the Small Magellanic Cloud (SMC) are gas-rich dwarf irregular galaxy satellites of the Milky Way (MW). The Magellanic Clouds (MCs) and the MW represent the closest group of interacting galaxies, providing the best opportunity to investigate satellite–satellite and satellite–host galaxy gravitational interactions (see e.g. D'Onghia & Fox 2016). Moreover, the MCs are fundamental benchmarks in the context of stellar populations and galactic evolution studies (see e.g. Harris & Zaritsky 2004, 2009; Ripepi et al. 2014b, and references therein). Indeed, they are fairly close ($D \sim 50$–60 kpc; de Grijs, Wicker & Bono 2014; de Grijs & Bono 2015), host stellar populations of diverse ages/metallicities and their morphologies were notably affected by the dynamical interaction between them and with the MW.

There are clear signatures that the SMC is interacting with both the LMC and the MW. In particular, the MCs are connected by a Magellanic Bridge (MB) traced by H I gas but also including a significant stellar content (e.g. Irwin, Kunkel & Demers 1985; Harris 2007). Like the Magellanic Stream (MStr), an H I structure embracing the MCs and extending over a large region of the sky, the MB may be the signature of the MCs' mutual gravitational interaction and/or the impingement of the MW (e.g. Putman et al. 1998; Hammer et al. 2015). Furthermore, the SMC Wing or Shapley Wing (Shapley 1940), extending asymmetrically towards the LMC, could be the result of tidal interaction(s). Additionally, the asymmetric and elongated SMC shape, especially when traced by the young population, reveals the strength of the gravitational forces acting between the two Clouds.

Very recent investigations of MCs' outskirts revealed a perhaps more complex structure of the whole Magellanic system (MS), including either relics of its formation or the results of strong tidal interaction between the MCs. Indeed (i) a number of ultrafaint dwarf galaxies, recently discovered in the Dark Energy Survey (DES), might be associated with the LMC (Deason et al. 2015; Drlica-Wagner et al. 2015, 2016; Koposov et al. 2015; Jethwa, Erkal & Belokurov 2016; Martin et al. 2016; Sales et al. 2017); (ii) a stellar protuberance extending by about 10 kpc was discovered by Mackey et al. (2016) within the LMC's tidal radius; (iii) Belokurov et al. (2017) used *Gaia* satellite data release 1 (Gaia Collaboration 2016a,b) to reveal that the LMC and SMC tidal arms are stretched towards each other to form an almost continuous (new) stellar bridge; (iv) a stellar overdensity called Small Magellanic Cloud Northern Over-Density (SMCNOD) was discovered 8° north (N) of the SMC centre by Pieres et al. (2017) on the basis of DES, Survey of the MAgellanic Stellar History (SMASH) and MAGellanic SatelLITEs Survey (MagLiteS) data. These new findings show that perhaps the inventory of the MS is still incomplete.

In this context, recent studies based on proper motion estimates, using *Hubble Space Telescope* (*HST*) and *Gaia* satellite data, suggest that the MCs are at their first passage of the MW (Besla et al. 2007; Kallivayalil et al. 2013; van der Marel & Sahlmann 2016, and references therein). This suggests that both the MStr and MB are the result of strong interactions between the two Clouds before they interacted with the MW. Furthermore, simulations by Diaz & Bekki (2012) predict close encounters ∼2 Gyr and ∼200 Myr ago, leading to the formation of the MStr and MB, respectively. The same models also predict the existence of a Counter-Bridge (CB) in the opposite direction to the MB. Other models (Besla et al. 2012) reproduce the formation of the MStr, the off-centre bar of the LMC and the formation of the MB, this last under the hypothesis of an impact between the MCs at an epoch between 100 and 300 Myr ago.

Focusing on the SMC, it is commonly thought that this galaxy is composed of two components: (i) young stars and H I gas forming a disc; (ii) old and intermediate-age populations more smoothly distributed in a spheroid or ellipsoid (see e.g. Caldwell & Coulson 1986; Gardiner & Noguchi 1996; Cioni, Habing & Israel 2000; Zaritsky et al. 2000; Maragoudaki et al. 2001; Stanimirović, Staveley-Smith & Jones 2004; Harris & Zaritsky 2006; Bekki & Chiba 2008; Evans & Howarth 2008; Glatt et al. 2008; Gonidakis et al. 2009; Haschke, Grebel & Duffau 2012; Subramanian & Subramaniam 2012, 2015; Rubele et al. 2015, among others). A common finding among many of the quoted works is that the north-eastern region of the bar/disc is closer to us than its south-western part (as early-on recognized by Welch et al. 1987; Hatzidimitriou & Hawkins 1989). Moreover, the SMC shows a considerable line-of-sight (LOS) depth whose precise quantitative extent depends on the methods and tracers used for the measure spanning a few kpc to more than 20 kpc (see e.g. de Grijs et al. 2014, for a review).

Our view of the SMC and its interaction with its neighbour has changed significantly in recent years. Nidever et al. (2013) used Washington photometry of Red Clump (RC) stars in eight MOSAIC@CTIO-4m fields to identify a stellar structure significantly closer to us ($D \sim 55$ kpc) than the main body of the SMC (placed at $D \sim 67$ kpc in that work), in its eastern part (around 4.2 kpc from SMC centre). They interpret this structure as a component which was tidally stripped during the last interaction with the LMC (∼200 Myr ago). Using synthetic colour–magnitude diagram (CMD) fitting technique, Noël et al. (2015) suggest that the intermediate-age population in the region of the MB closer to the SMC was tidally stripped from the galaxy, as its properties are similar to those of the intermediate-age stellar populations in the inner regions of the galaxy. From a kinematic investigation of Red Giants in the SMC, Dobbie et al. (2014) found the presence of tidally stripped stars associated with the MB.

More recently, on the basis of the VISTA[1] near-infrared YJK_s survey of the Magellanic Clouds system (VMC; Cioni et al. 2011, see below), Subramanian et al. (2017) identified a foreground population (∼11.8 ± 2.0 kpc in front of the main body), whose most likely explanation is tidal stripping from the SMC. Moreover, they identify the inner region (∼2–2.5 kpc from the centre) from where the signatures of interactions start becoming evident, thus supporting the hypothesis that the MB was formed from tidally stripped material from the SMC.

As for the detailed three-dimensional structure of the SMC, the classical pulsating stars, RR Lyrae and Classical Cepheids (CCs), have been widely used in the literature as distance indicators and tracers of the old (age >10 Gyr) and young (age typically ∼50–500 Myr) populations, respectively. Concerning RR Lyrae, very recent investigations based on both near-infrared (NIR) time-series data (VMC survey) and optical OGLE IV survey data (Udalski et al. 2015a) found that the distribution of old pulsators in the SMC has an ellipsoidal shape, with a significant LOS depth (∼1–10 kpc) devoid of any particular substructure, though with some asymmetry in the eastern–south-eastern region of the SMC (i.e. roughly in the direction of the LMC) which appears to be closer to us (Subramanian & Subramaniam 2012; Deb et al. 2015; Jacyszyn-Dobrzeniecka et al. 2017; Muraveva et al. 2017).

[1] Visible and Infrared Survey Telescope for Astronomy.

Using *Spitzer* mid-infrared time-series photometry of 92 bright CCs in the SMC, Scowcroft et al. (2016) confirmed that the galaxy is tilted and elongated, with its eastern side up to 20 kpc closer than the western one. In addition, they suggested that the investigated CCs are not distributed on a disc, but rather have a cylindrical shape. Scowcroft et al. (2016)'s results also seem to support the hypothesis of a direct collision between the MCs to explain the fact that the objects closer to each Cloud when projected on the sky are also physically closer to each other. More recently, Jacyszyn-Dobrzeniecka et al. (2016) presented a thorough investigation of the three-dimensional structure of the MCs based on OGLE IV optical time-series data for thousands of CCs in both Clouds. They confirmed Scowcroft et al. (2016)'s results, i.e. the SMC CCs do not have a disc-like distribution, but their structure can be described as an extended ellipsoid. In addition, they identified two large ellipsoidal off-axis structures. The northern one is located closer to the Sun and it is younger, whereas the south-western structure is more distant and older. Jacyszyn-Dobrzeniecka et al. (2016), confirming Subramanian & Subramaniam (2015)'s earlier results, found that the age distribution of the CCs in the SMC is almost bimodal with two peaks at 110 and 220 Myr (an average error of ∼20 Myr is provided by Subramanian & Subramaniam 2015). According to their results, younger pulsators are located in the closer region of the SMC whereas older ones are more distant. These authors also associate nine CCs with the MB, finding that all of them are younger than ∼300 Myr, in agreement with current theories about the formation of the MB, which foresee that young stars in MB are the result of *in situ* star formation from the tidally stripped material from the SMC.

In this paper, we exploit the YJK_s time-series photometry collected in the context of the VMC survey for a sample of CCs in the SMC including 97.5 per cent (see below) of the known pulsators of this class in this galaxy. The techniques adopted (template fitting) for the photometry and the average magnitudes for 4172 SMC CCs were presented by Ripepi et al. (2016, Paper I). This work enlarges the sample of investigated CCs by 15 per cent (see the next section). In Paper I, we adopted our high-precision photometry (complemented with literature V magnitudes) to construct a variety of period–luminosity (*PL*), period–luminosity–colour (*PLC*) and period–Wesenheit (*PW*) relationships, valid for Fundamental (F), First Overtone (1O) and Second Overtone (2O) pulsators (the first relation to date for this mode of pulsation). The *PW* was used to estimate the distance to the SMC relative to the LMC and, in turn, the absolute distance to the SMC. We found $\Delta\mu = 0.55 \pm 0.04$ mag for the relative distance and $\mu_{\rm SMC} = 19.01 \pm 0.05$ mag or $\mu_{\rm SMC} = 19.04 \pm 0.06$ mag for the absolute value. The two estimates rely on two different distance measurements to the LMC: accurate CC and eclipsing Cepheid binary data, respectively.

The scope of this work is to take advantage of the high-precision NIR *PW* to estimate accurate single relative distances for each CC in the SMC, and, in turn, use these data to reveal the 3D structure of the SMC over an area of more than 40 deg^2 covering entirely the SMC body and large parts of its outskirts. The advantage of our data with respect to, e.g. Scowcroft et al. (2016) is that we have a comparable precision in the photometry but an incomparably larger sample. As for the work by Jacyszyn-Dobrzeniecka et al. (2016), we have a comparable sample size, but a higher precision of the single CC distances. Indeed, going to the NIR has several advantages for the CCs as amplitudes are much smaller than in the optical bands, and hence accurate average magnitudes can be obtained using a smaller number of epochs along the pulsation cycle with respect to the optical bands. A particular advantage of the *PW* using the (V, K_s) bands is that the colour coefficient is the same as that of the *PLC*. This means that the *PW* for this particular combination of colours is not only reddening-free and mildy metallicity dependent (see e.g. Caputo, Marconi & Musella 2000), but also devoid of the uncertainties due to the finite width of the instability strip affecting the *PL* relations and to a lesser extent the *PW* ones.

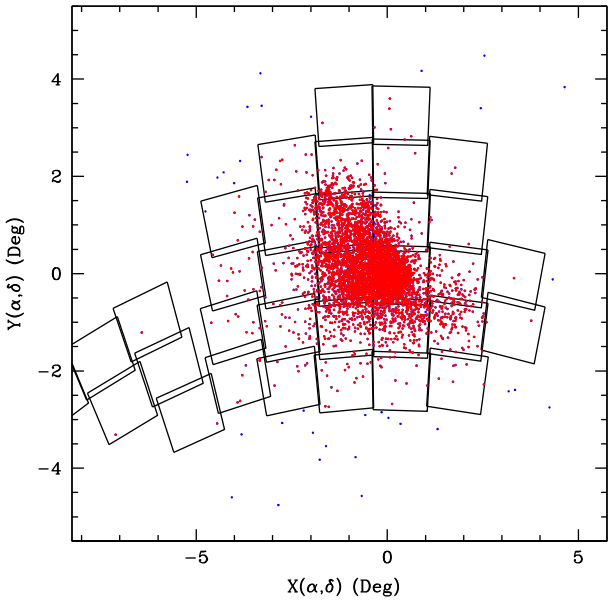

Figure 1. Map of the CCs in the SMC. Red and blue circles show CCs in the OGLE IV survey with and without counterparts in the VMC survey, respectively. The solid rectangles show the location of the VMC tiles. The centre is at $\alpha_0 = 12.54$ deg; $\delta_0 = -73.11$ deg.

This paper is organized as follows: Section 2 presents the observations and the analysis of the CCs' light curves; Section 3 illustrates the construction of the new *PL* and *PW* relationships obtained in this paper from the enlarged sample of CCs; in Section 4, we find individual distances to CCs in the SMC and discuss their 3D distribution; Section 5 presents a discussion of the results, while Section 6 briefly summarizes the main outcomes of this paper.

2 SMC CLASSICAL CEPHEIDS IN THE VMC SURVEY

The list of CCs in the SMC used as reference was taken from the OGLE IV survey (Soszyński et al. 2015a,b; Udalski et al. 2015b), whose results supersede those of the OGLE III (Soszyński et al. 2010) and EROS 2 (Tisserand et al. 2007) surveys used in Paper I. In more detail, OGLE IV published the identification, the V, I light curves and main properties (periods, mean magnitudes, amplitudes etc.) for 4915 CCs in the SMC.[2]

The area observed by the VMC survey in the region of the SMC is shown in Fig. 1, where each square represents one VMC tile (each tile is 1.65 deg^2 on the sky). In this paper, we present results for the CCs included in 31 tiles completely or nearly completely observed, processed and catalogued by the VMC survey as of 2016 August 22 (including observations until 2016 March 31). The cross-match between the OGLE IV CCs and VMC sources with at least six epochs

[2] Note that Soszyński et al. (2015a) estimated the OGLE IV collection of CCs in the MCs is complete at least at the 99 per cent level.

in K_s (sufficient to obtain very precise magnitudes) within a radius of 0.5 arcsec returned 4784 matches. Of the 131 missing objects, 55 are located outside of the VMC tiles or in the gap between tiles SMC 5_3 and 5_4,[3] whereas for the remaining 76 we enlarged the search radius to 2 arcsec and inspected the light curve of the closest matching star, as well as the actual position of the targets on the VMC images. As a result, we recovered nine additional CCs with usable light curves, while the remaining 67 objects showed unusable data due to different causes, such as blending, too few epochs (vicinity to borders of the tile) and saturation. After this procedure, the total number of stars with usable light curves contains 4793 objects, which represent the 97.5 per cent of the OGLE IV sample. The classification of the targets in terms of pulsation modes was also taken from OGLE IV. Our sample counts 2684, 1729, 90 and 290 F, 1O, 2O, and mixed modes (F/1O, 1O/2O, F/1O/2O, 1O/2O/3O, where TO stands for Third Overtone) CCs, respectively. Note that with respect to Paper I, the sample analysed here is significantly larger (∼720 additional CCs) and more accurate because (i) OGLE IV covers a larger area with respect to OGLE III and EROS 2; (ii) OGLE IV reclassified with different variable types 32 and 10 objects originally classified as CCs in OGLE III and EROS 2, respectively. In total, the present sample has 4076 stars in common with that of Paper I.

A general description of the observations in the context of the VMC survey can be found in Cioni et al. (2011), whereas the procedures adopted to study the variable stars were discussed in detail in Paper I and in Ripepi et al. (2012a,b, 2014a, 2015), Moretti et al. (2014, 2016), Muraveva et al. (2014, 2015), Marconi et al. (2017). Therefore, here we only briefly recall that the VMC K_s-band time-series observations were programmed to span 13 separate epochs executed over several consecutive months. This observing strategy allowed us to obtain well-sampled light curves for the relevant pulsating stars. As for the Y and J bands, the planned number of epochs is four (two of these epochs are obtained with half exposure times). However, additional observations (a few epochs) are usually available for each tile (in particular for the K_s band) because some observing blocks (OBs) executed out of specifications provided usable data. Additionally, the overlap between the tiles and the high density of CCs in the body of the SMC cause the presence of many CCs in two or more different tiles and consequently about 490 CC light curves are sampled with more than 23 epochs. The situation is similar in the Y and J bands, and the number of CCs with more than 10 epochs is 232 and 404 in the Y and J filters, respectively (see Paper I for more details). Again, there are some differences with respect to Paper I, as additional VMC observations were obtained and fully reduced since the time of the writing of Paper I. As a result, considering the sample in common with Paper I, we have now 40 pulsators with approximately twice the number of planned epochs in the YJK_s bands. In addition, 1229 stars have one epoch more in K_s, while 243 objects show between two and five additional epochs again in the K_s. As we shall see in what follows, the availability of additional epochs of observations for a subsample of pulsators can lead to slight differences in the measurements of their magnitudes.

The data analysed in this paper were processed by means of the pipeline of the VISTA Data Flow System (VDFS; Emerson et al. 2004; Irwin et al. 2004). The photometry is in the VISTA photometric system (Vegamag = 0; the VISTA photometric system is described by González-Fernández et al. 2017). The time-series data used in this work were downloaded from the VISTA Science Archive[4] (VSA, Cross et al. 2012). More details about the characteristics of CC time-series such as those used in this paper can be found in Paper I.

The VMC light curves in the Y, J and K_s filters of the 717 CCs analysed in this paper and not present in Paper I are shown in Appendix A. Similarly, in Table 1, we publish the VMC photometry for these 757 variables (including the quoted 40 variables having almost twice epochs with respect to Paper I). The complete versions of the table and of the figures are available online on the journal's site.

Table 1. Y, J and K_s time-series photometry for the 757 CCs investigated in this paper (see the text). The sample data below refer to the variable OGLE-SMC-CEP-3294.

HJD-2 400 000	Y	σ_Y
55492.59442	16.142	0.005
55492.62957	16.154	0.005
55497.70358	16.006	0.005
55539.61982	15.867	0.005
HJD-2 400 000	J	σ_J
55493.58657	15.783	0.005
55493.62563	15.792	0.005
55495.55133	15.912	0.007
55539.63935	15.698	0.006
55778.75250	15.811	0.006
HJD-2 400 000	K_s	σ_{K_s}
55493.78578	15.592	0.010
55495.57476	15.649	0.013
55495.68414	15.627	0.010
55497.72311	15.553	0.011
55538.61986	15.564	0.010
55549.58433	15.561	0.010
55769.75246	15.650	0.011
55778.77203	15.586	0.012
55791.76028	15.601	0.010
55818.72858	15.640	0.011
55820.67384	15.540	0.009
55879.55444	15.552	0.010
55880.61689	15.541	0.011
55900.56920	15.634	0.010
56130.79148	15.599	0.010
56173.70146	15.579	0.011
56195.63840	15.546	0.009
56223.53971	15.604	0.010

Table 1 is published in its entirety only in the electronic edition of the journal. A portion is shown here for guidance regarding its form and content.

3 AVERAGE MAGNITUDES AND *PL*/*PW* RELATIONS

We estimated the Y, J and K_s intensity-averaged magnitudes and the peak-to-peak amplitudes for the full sample of 4793 CCs adopting the same techniques as in Paper I. In brief, we constructed eight different templates for each of the three Y, J and K_s bands and used a modified χ^2 technique to identify the best-fitting template. To estimate the uncertainties on the mean magnitudes and the peak-to-peak amplitudes, we adopted a Monte Carlo technique consisting

[3] Note that this gap will be filled with ad hoc observations already approved by ESO; proposal 099.D-0194.

[4] http://horus.roe.ac.uk/vsa/

Table 2. Photometric results for all the 4793 CCs analysed in this paper. Columns: (1) identification from OGLE IV; (2) mode: F = Fundamental; 1O = First Overtone; 2O = Second Overtone; 3O = Third Overtone; (3) VMC tile in which the object is found; (4) period; (5) number of epochs in Y; (6) and (7) intensity-averaged magnitude in Y and relative uncertainty; (8) and (9) peak-to-peak amplitude in Y and relative uncertainty; (10)–(14) as for columns (5)–(9) but for the J band; (15)–(19) as for columns (5)–(9) but for the K_s band; (20) $E(V-I)$ values adopted in this work.

OGLE_ID	Mode	VMC tile	P	n_Y	$\langle Y\rangle$	$\sigma_{\langle Y\rangle}$	$A(Y)$	$\sigma_{A(Y)}$	n_J	$\langle J\rangle$	$\sigma_{\langle J\rangle}$	$A(J)$	$\sigma_{A(J)}$	n_{K_s}	$\langle K_s\rangle$	$\sigma_{\langle K_s\rangle}$	$A(K_s)$	$\sigma_{A(K_s)}$	$E(V-I)$
			(d)		(mag)	(mag)	(mag)	(mag)		(mag)	(mag)	(mag)	(mag)		(mag)	(mag)	(mag)	(mag)	(mag)
(1)	(2)	(3)	(4)	(5)	(6)	(7)	(8)	(9)	(10)	(11)	(12)	(13)	(14)	(15)	(16)	(17)	(18)	(19)	(20)
OGLE-SMC-CEP-2476	1O	SMC_5_4	0.2526028	4	19.055	0.072	0.11	0.09	5	18.875	0.033	0.16	0.07	18	18.696	0.046	0.120	0.054	0.05
OGLE-SMC-CEP-3867	1O/2O/3O	SMC_4_4	0.2688496	4	18.454	0.022	0.19	0.03	5	18.247	0.019	0.14	0.03	15	18.033	0.033	0.050	0.048	0.05
OGLE-SMC-CEP-2507	1O/2O	SMC_4_4	0.2775568	4	18.651	0.017	0.07	0.04	5	18.428	0.022	0.07	0.04	15	18.206	0.041	0.197	0.084	0.03
OGLE-SMC-CEP-2752	1O	SMC_4_4	0.2837457	8	17.954	0.011	0.12	0.03	10	17.809	0.011	0.15	0.02	33	17.683	0.016	0.100	0.026	0.11
OGLE-SMC-CEP-2095	1O	SMC_5_3	0.2870474	5	18.129	0.016	0.33	0.02	9	17.918	0.009	0.18	0.04	19	17.774	0.019	0.064	0.039	0.03
OGLE-SMC-CEP-0022	1O	SMC_4_2	0.3136645	5	18.445	0.019	0.18	0.03	5	18.268	0.016	0.10	0.02	15	18.057	0.033	0.099	0.053	0.02
OGLE-SMC-CEP-4548	1O	SMC_5_5	0.3247217	5	18.402	0.019	0.13	0.03	4	18.245	0.027	0.12	0.02	14	18.164	0.029	0.133	0.054	0.03
OGLE-SMC-CEP-1471	1O/2O	SMC_5_3	0.3271798	5	17.726	0.011	0.11	0.01	9	17.544	0.007	0.11	0.02	19	17.327	0.014	0.062	0.021	0.03
OGLE-SMC-CEP-2527	1O/2O	SMC_4_4	0.3292266	4	18.173	0.024	0.07	0.03	5	17.941	0.015	0.06	0.02	15	17.676	0.027	0.100	0.046	0.03
OGLE-SMC-CEP-2683	1O	SMC_4_4	0.3373664	4	18.045	0.011	0.10	0.02	5	17.751	0.013	0.02	0.02	15	17.350	0.021	0.070	0.007	0.05
OGLE-SMC-CEP-3287	1O	SMC_4_4	0.3464235	4	18.061	0.017	0.14	0.04	5	17.876	0.016	0.11	0.03	15	17.677	0.023	0.131	0.035	0.04
OGLE-SMC-CEP-4242	1O	SMC_4_4	0.3465840	4	17.859	0.008	0.06	0.02	5	17.563	0.010	0.06	0.02	15	17.157	0.013	0.076	0.026	0.05
OGLE-SMC-CEP-1606	1O/2O	SMC_4_3	0.3525089	6	18.310	0.018	0.20	0.04	6	18.073	0.019	0.12	0.04	16	17.784	0.027	0.070	0.030	0.02
OGLE-SMC-CEP-4628	1O	SMC_3_5	0.3643637	7	17.390	0.006	0.05	0.01	5	17.106	0.007	0.02	0.01	16	16.642	0.009	0.016	0.011	0.05
OGLE-SMC-CEP-3784	1O	SMC_4_4	0.3803699	4	18.275	0.047	0.18	0.02	5	18.007	0.015	0.19	0.03	15	17.745	0.025	0.090	0.036	0.03
OGLE-SMC-CEP-3660	1O/2O	SMC_4_4	0.3867429	4	16.895	0.008	0.12	0.01	5	16.539	0.006	0.08	0.01	15	16.136	0.006	0.034	0.013	0.05
OGLE-SMC-CEP-4243	1O	SMC_4_4	0.3937253	4	18.126	0.012	0.28	0.03	5	17.909	0.012	0.14	0.03	15	17.642	0.019	0.068	0.036	0.09
OGLE-SMC-CEP-0310	1O	SMC_4_3	0.3942412	6	17.896	0.015	0.19	0.06	6	17.703	0.012	0.16	0.03	16	17.531	0.019	0.150	0.033	0.06
OGLE-SMC-CEP-1357	2O	SMC_4_3	0.4012875	6	17.701	0.010	0.04	0.02	6	17.461	0.011	0.03	0.02	16	17.256	0.015	0.043	0.025	0.05
OGLE-SMC-CEP-2265	1O	SMC_3_3	0.4085550	7	17.824	0.015	0.13	0.03	5	17.688	0.017	0.21	0.02	18	17.500	0.017	0.100	0.032	0.03

Table 2 is published in its entirety in the electronic edition of the MNRAS. A portion is shown here for guidance regarding its form and content.

of the generation of 100 mock time-series for each star and each filter, to which Gaussian noise was added with standard deviations σs corresponding to the average errors on the phase points for the target star. At variance with Paper I, we decided to use the Monte Carlo simulations to estimate not only the errors on the amplitudes in the three bands, but also the actual amplitudes, by averaging the amplitudes resulting from the 100 experiments.

We did not use the simulation to estimate the intensity-averaged magnitudes (but only the uncertainties on their values) because we verified that the difference between the magnitudes obtained from the best fit and those estimated as the average of the 100 simulations, agree very well within the uncertainties. This is because the magnitudes estimated with the templates are only mildly affected by even large errors in the estimated amplitudes, an occurrence that can happen when we have only four to six epochs in the light curves (e.g. in the Y, J bands).

The result of these procedures is shown in Table 2, which is available in its entirety associated with the online version of the paper.

Fig. 2 shows the difference between the present and Paper I photometry for the 4076 stars in common. It can be seen that for the vast majority of the stars the difference in magnitude and amplitude is well below 0.01 mag. Fig. 3 gives an idea of the typical errors as a function of the magnitudes for the whole sample of 4793 CCs.

The intensity-averaged magnitudes thus obtained were used to construct new *PL* and *PW* relations including the new CCs. These relations will be at the basis of our structural analysis of the SMC. Before proceeding, we have to calculate the dereddened Y, J and K_s magnitudes. The last column of Table 2 reports the individual colour excesses $E(V-I)$ derived according to Haschke, Grebel & Duffau (2011). For the CCs located outside the region investigated by those authors (i.e. the area covered by the OGLE III survey), we adopted a mean value of $E(V-I) = 0.035$ mag, calculated averaging the $E(V-I)$ values obtained for the CCs inside the area covered by OGLE III. For the extinction corrections, as in Paper I, we used Cardelli, Clayton & Mathis (1989), Kerber et al. (2009) and Gao et al. (2013).

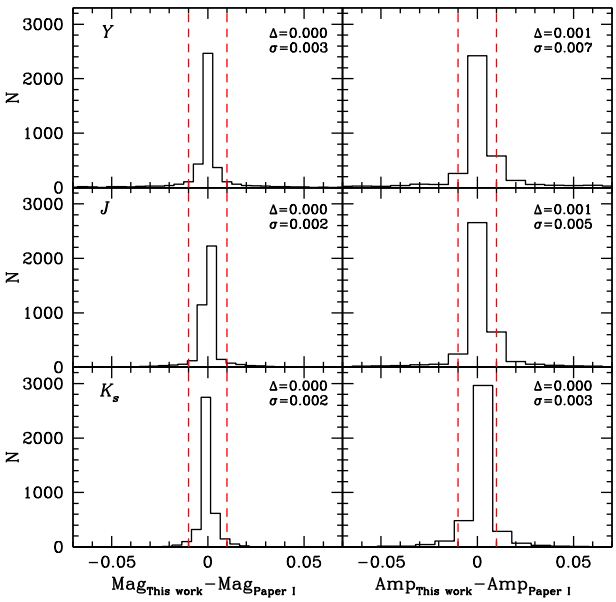

Figure 2. Left-hand panels: comparison between the intensity-averaged magnitudes obtained in this work and those of Paper I. Right-hand panels: same as left-hand panels but for the amplitudes. In all panels, the dashed lines show the ± 0.01 mag limits. The bins widths are 0.005 and 0.01 mag for the magnitudes and amplitudes, respectively. Each panel shows the average difference (Δ) and the relative dispersion (σ), calculated with a 3σ clipping procedure.

As discussed in detail in Paper I, we fitted two relations to the F-mode pulsators because of the presence of a change in slope at period ∼ 2.95 d. We chose not to recalculate the *PLC* relations because they are substantially very similar to the *PW* relations [almost identical in the case of the $PW(V, K_s)$]. With respect to Paper I, we used a slightly different technique to perform the least-squares fit to the data. Specifically, we applied to all relations a sigma-clipping algorithm, fixing 3.5σ. This approach guarantees repeatability of

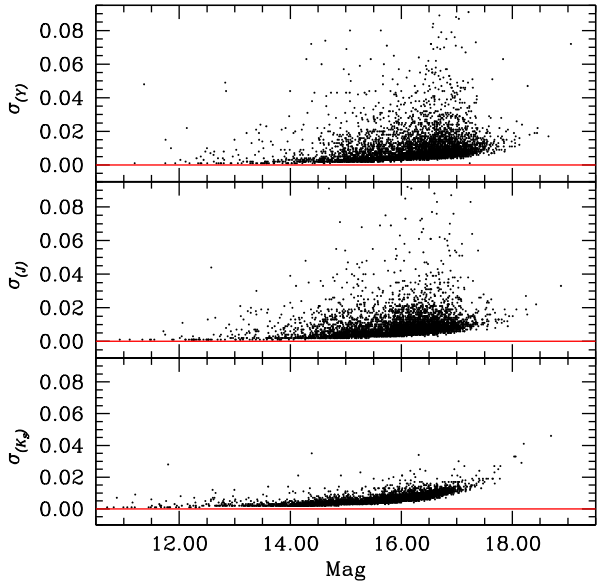

Figure 3. Uncertainties in our photometry according to the Monte Carlo simulations.

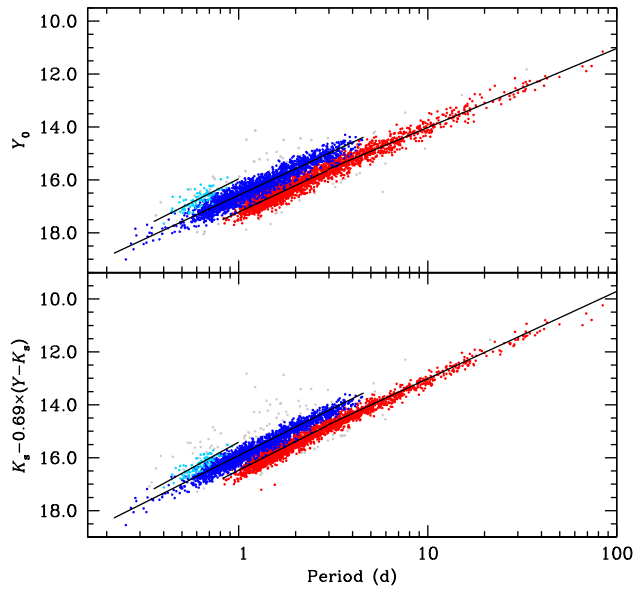

Figure 4. *PL*(*Y*) and *PW*(*K*$_s$, *Y*) relations for the SMC CCs investigated in this paper. F, 1O and 2O pulsators are shown as red, blue and light blue filled circles, respectively. The grey filled circles show objects excluded from the analysis because they deviate more than 3.5σ from the best fits to the data represented by solid lines.

the procedure and avoids excluding stars that could be off the ridge-line due to their position and not to photometric problems. The results of these procedures are shown in Figs 4–6 and in Table 3. A comparison between Table 3 and table 6 of Paper I shows that the parameters of the *PL* and *PW* relations (and relative uncertainties) agree within the errors.

4 THE 3D STRUCTURE OF THE SMC YOUNG POPULATION

The scope of this section is to determine the three-dimensional structure of the young population of the SMC as traced by the

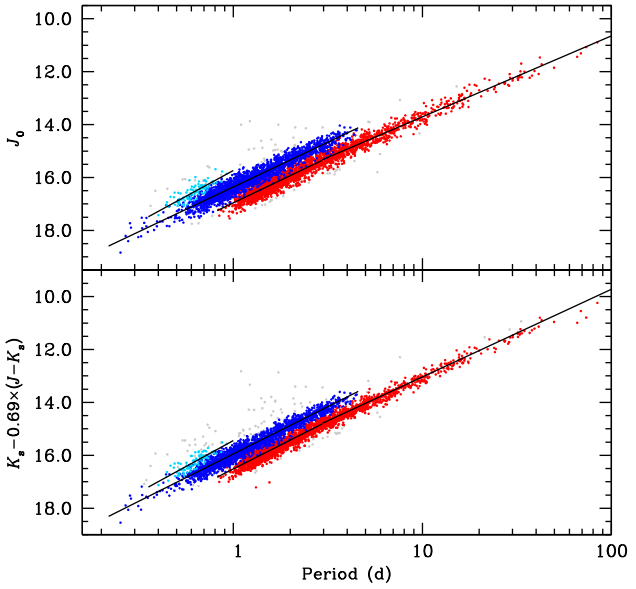

Figure 5. As in Fig. 4, but for the *J* filter.

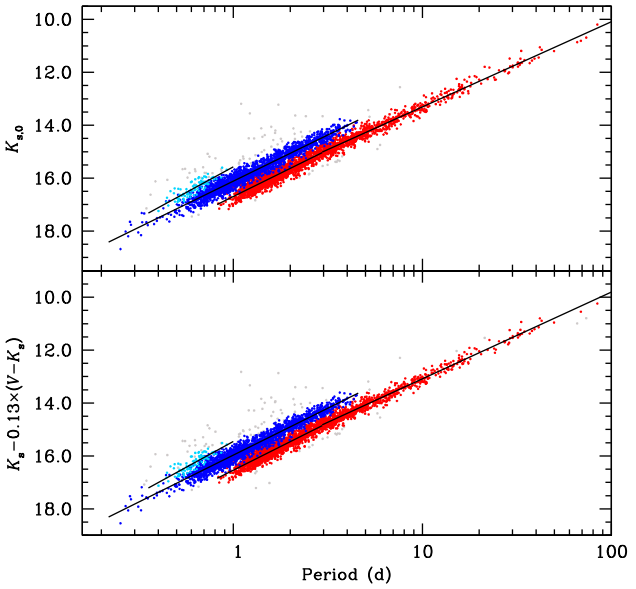

Figure 6. As in Fig. 4, but for the *V* filter.

CCs. The first step is to estimate the relative distances of each CC with respect to the centre of the distribution of the CCs in the SMC (note that the centre of the SMC is poorly defined, see discussion in de Grijs & Bono 2015). To this aim, we produced a smoothed 2D histogram in the equatorial coordinates α, δ of the studied variables using a box-smoothing area of $0.20\times0.20\,\mathrm{deg}^2$ (but the result is only mildly dependent on this choice), as shown in Fig. 7. This figure reveals that the spatial distribution of the CCs is rather asymmetric and to determine its centre we calculated the average α, δ using only the bi-dimensional bins containing more than 60 counts (we verified that the result is not significantly affected by this choice). The resulting centre is $\alpha_0 = 12.54 \pm 0.01$ deg and $\delta_0 = -73.11 \pm 0.01$ deg, the uncertainties are the rms of the mean. This result is compared with the literature in Table 4. Our result is compatible with those estimated from the density of the stars (Gonidakis et al. 2009; Rubele et al. 2015) and consistent in δ but

Table 3. *PL* and *PW* relations for F, 1O and 2O CCs. The Wesenheit functions are defined in the table.

Mode	a	σa	b	σb	rms
		$Y^0 = a\log P + b$			
F $\log P < 0.47$	−3.353	0.041	17.216	0.010	0.202
F $\log P \geq 0.47$	−2.987	0.027	17.008	0.021	0.202
1O	−3.321	0.023	16.582	0.005	0.215
2O	−3.572	0.305	15.964	0.068	0.205
		$J^0 = a\log P + b$			
F $\log P < 0.47$	−3.406	0.041	16.952	0.010	0.206
F $\log P \geq 0.47$	−3.070	0.026	16.778	0.021	0.196
1O	−3.377	0.021	16.356	0.005	0.203
2O	−3.602	0.308	15.776	0.069	0.207
		$K_s^0 = a\log P + b$			
F $\log P < 0.47$	−3.513	0.036	16.686	0.009	0.177
F $\log P \geq 0.47$	−3.224	0.023	16.530	0.018	0.167
1O	−3.489	0.020	16.112	0.005	0.186
2O	−3.989	0.317	15.520	0.070	0.208
		$W(Y, K_s) = K_s - 0.42\,(Y - K_s) = a\log P + b$			
F $\log P < 0.47$	−3.608	0.033	16.473	0.008	0.165
F $\log P \geq 0.47$	−3.296	0.020	16.308	0.016	0.149
1O	−3.577	0.018	15.918	0.004	0.173
2O	−3.914	0.271	15.415	0.060	0.174
		$W(J, K_s) = K_s - 0.69\,(J - K_s) = a\log P + b$			
F $\log P < 0.47$	−3.597	0.034	16.504	0.009	0.169
F $\log P \geq 0.47$	−3.334	0.021	16.363	0.017	0.158
1O	−3.572	0.019	15.945	0.004	0.179
2O	−4.060	0.353	15.374	0.078	0.232
		$W(V, K_s) = K_s - 0.13\,(V - K_s) = a\log P + b$			
F $\log P < 0.47$	−3.567	0.034	16.527	0.009	0.170
F $\log P \geq 0.47$	−3.291	0.021	16.375	0.017	0.155
1O	−3.544	0.019	15.967	0.004	0.178
2O	−3.790	0.344	15.438	0.077	0.231

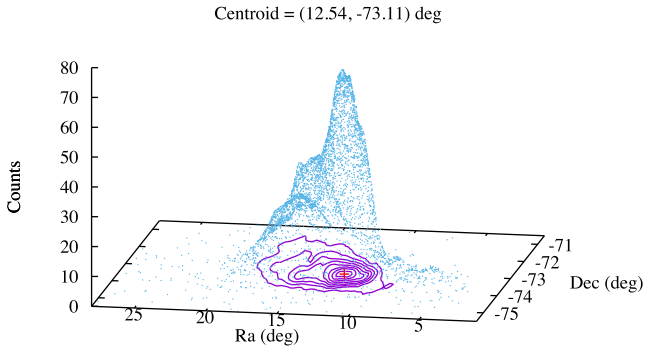

Figure 7. Bi-dimensional histogram of the spatial distribution in α, δ of CCs in the SMC. The contour levels span the range 0–40 counts with an interval of 5 counts between each level. A cross marks the chosen centre of the distribution.

differing by about 1 deg in α from the previous values inferred from the distribution of RR Lyrae and CCs variables (Subramanian & Subramaniam 2012, 2015, respectively).

The next step is to find the relative distances of each CC with respect to this centre. To this aim, we decided to use only the *PW* relations derived in the previous section, because (i) they are intrinsically more accurate with respect to the *PL* relations; (ii) they are independent of reddening; (iii) especially in the case of $W(V, K_s)$, the colour term is very similar to that of the *PLC* relations (see e.g. Ripepi et al. 2012b, and Paper I), which should, in principle, show a negligible dispersion (see e.g. Bono et al. 1999).

We first calculated the magnitude difference between all CC and the *PW* relations:

$$\Delta W(\lambda_1, \lambda_2)_i = W(\lambda_1, \lambda_2)_i - (\alpha + \beta \log P), \quad (1)$$

where (λ_1, λ_2) can assume the value of (V, K_s) or (J, K_s) and the relative α and β values are listed in Table 3. To transform these ΔW values into absolute distances, we adopted the distance modulus of the SMC we estimated in Paper I, distance modulus $\mu = 19.01$ mag corresponding to $D_{SMC} = 63$ kpc. The precise value of this quantity does not affect the subsequent analysis (see e.g. Subramanian & Subramaniam 2015). The individual distances are hence calculated as

$$D_i = D_{SMC} 10^{(\Delta W_i/5)} \quad (2)$$

As for the errors on the individual relative distances, the photometric errors are shown in Fig. 3. For the large majority of the CCs, they are less than 0.02 mag in Y and J, and less than 0.01 mag in K_s. This translates at the distance of the SMC in ∼0.6 and 0.3 kpc, respectively. When using the *PW* relations, the photometric errors are summed in quadrature and become of the order of 0.65 kpc for all combinations of colours used in this work (we adopted an uncertainty of 0.02 mag for the OGLE IV Johnson V band; see Jacyszyn-Dobrzeniecka et al. 2016). The possible inaccuracy of the reddening law chosen to construct the *PW* relations could in principle be an additional cause of uncertainty, but the coefficients are very small in the NIR and this contribution is hence negligible. However, the intrinsic dispersion of the various relations adopted can represent the major source of error. Any *PL*, *PW* or *PLC* has an intrinsic dispersion, due to e.g. the finite width of the instability strip, mass-loss, rotation and differences in metallicity. The major contributor to the intrinsic dispersion is certainly the finite width of the instability strip, which affects significantly the *PL* (even though in NIR bands the effect is reduced). This effect is much reduced for *PW* relations. In our case, the most accurate relations at our disposal are the $PW(J, K_s)$ and $PW(V, K_s)$. An estimate of the intrinsic dispersion in these relations is ∼0.04 and 0.05 mag, respectively, as reported by Inno et al. (2016), on the basis of the up-to-date theoretical scenario of Bono et al. (1999, 2010). Hence, summing up in quadrature all the sources of errors, our individual relative distance errors are ∼1.35 and 1.6 kpc (at the distance of the centroid of the SMC) for the $PW(J, K_s)$ and $PW(V, K_s)$, respectively.

Fig. 8 displays the histogram of the results obtained with the $W(V, K_s)$ [equation 2; very similar results are obtained with $PW(J, K_s)$]. It shows that there is no systematic difference between the distance distribution of F pulsators before/after the break and 1O pulsators.

Having estimated the individual distances, we are now able to calculate the Cartesian coordinates for the CCs investigated here. According to van der Marel & Cioni (2001), Weinberg & Nikolaev (2001) for each CC, we can write

$$X_i = -D_i \sin(\alpha_i - \alpha_0)\cos\delta_i,$$
$$Y_i = D_i \sin\delta_i \cos\delta_0 - D \sin\delta_0 \cos(\alpha_i - \alpha_0)\cos\delta_i,$$
$$Z_i = D \sin\delta_i \sin\delta_0 - D \cos\delta_0 \cos(\alpha_i - \alpha_0)\cos\delta_i,$$

where D_i is the distance to each CC calculated based on equation (2), (α_i, δ_i) and (α_0, δ_0) represent the RA and Dec. of each CC and the centroid of the sample, respectively. By construction, the X-axis is antiparallel to the RA axis, the Y-axis is parallel to the

Table 4. Comparison between the centre of the distribution of the SMC CCs found here and a compilation of literature centres for the SMC (see also de Grijs & Bono 2015, for a discussion about the definition of the centre of the SMC).

Ra_0	Dec_0	Method	Source
16.25	−72.42	Kinematics of H I	Stanimirović et al. (2004)
12.75	−73.1	Density of 2MASS K and M stars	Gonidakis et al. (2009)
13.38	−73.0	Density of RR Lyrae stars	Subramanian & Subramaniam (2012)
12.60	−73.09	Stellar density VMC	Rubele et al. (2015)
13.90	−72.98	Density of CCs (OGLE III)	Subramanian & Subramaniam (2015)
12.54	−73.11	Density of CCs (OGLE IV)	This work

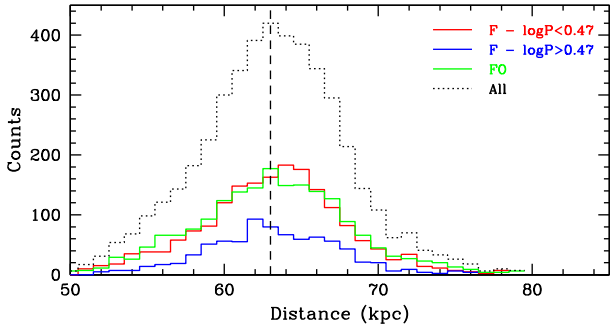

Figure 8. Distribution of the individual distances for the CCs analysed in this work as obtained by means of the $W(V, K_s)$ magnitude (see the text). The vertical dashed line shows the distance of the centroid of the SMC.

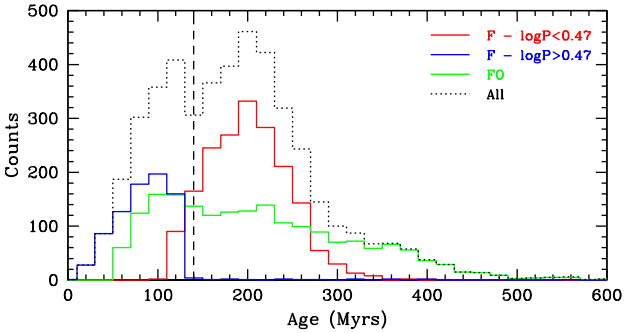

Figure 9. Distribution of the individual ages for the CCs analysed in this work as obtained by means of the *PAC* relations (after Bono et al. 2005). The vertical dashed line at 140 Myr is the boundary between young and old CCs.

declination axis and the *Z*-axis is towards the centroid of the SMC, i.e. increasing away from the observer.

4.1 Ages

An important ingredient for the following analysis is an estimate of the age of the CCs. This allows us to connect the pulsational properties of the CCs to those of the stellar population they belong to. This way we can use the position and the 3D structure of the CCs to infer that of the young population of the SMC, with typical ages of 10–500 Myr. The connection between the period and the age of a CC is rather obvious, given that the *PL* relations imply that at longer periods we have brighter objects. In turn, the mass–luminosity relation associated with this range of masses means that brighter objects have higher masses and hence younger ages. To estimate the ages of the investigated CCs, we adopted the period–age–colour (*PAC*) relations for F and 1O pulsators at $Z = 0.004$ of Bono et al. (2005); Marconi et al. (2006) (see also Anderson et al. 2016, for the possible effect of rotation on the age of CCs). The reliability of these relations has been confirmed in the literature (see e.g. the discussion in Subramanian & Subramaniam 2015). To calculate the $(V - I)_0$ colour needed in the *PAC* relations, we used OGLE IV V, I magnitudes and the reddening values listed in column 12 of Table 2. The resulting ages are in the range ∼10–900 Myr, with errors of the order of 5–30 Myr (larger errors for increasing ages). The result of this procedure is shown in Fig. 9. As already noted by Subramanian & Subramaniam (2015); Jacyszyn-Dobrzeniecka et al. (2016), the distribution is almost bimodal with two peaks at about 120(± 10) and 220 (±10) Myr. The bimodality of the distribution is almost entirely caused by F pulsators which are clearly separated depending on whether or not their periods place them before or after the break in the *PW* relations, respectively. The 1O pulsators appear to have a smoother distribution, encompassing the whole age range of the CC distribution.[5] Moreover, Fig. 9 shows two close main bursts of CCs, and the most recent one seems to have formed less stars.

We note that enhanced star formation rate (SFR) around 200 Myr (to 0 Myr) was shown in simulations (see e.g. fig. 7 in Yoshizawa & Noguchi 2003), but they did not show two clear peaks. Also, there is no decline in SFR between the two peaks. Hence, the observed bimodal age distribution among SMC CCs represents an important constraint for the next generation of simulations.

It is useful for the following analysis to divide the CCs into young and old samples, using 140 Myr as limiting age. This value is somewhat different from that adopted by Jacyszyn-Dobrzeniecka et al. (2016), as they used the Bono et al. (2005)'s period–age relations instead of the more precise *PAC* ones as we did here. However, this difference is not particularly significant for the following analysis.

4.2 Photometric metallicities

Metallicity, as well as age, is an important ingredient in the study of stellar populations. Extensive high-resolution spectroscopic surveys of CCs in the SMC are not available as the current instruments do not allow to carry out such measurements (this will be possible in the future with e.g. 4MOST@VISTA). It is however possible to obtain an estimate of the CCs' iron content based on the shape (Fourier parameters) of their light curves, as demonstrated by Klagyivik et al. (2013), who found multiband relationships connecting [Fe/H] with the R_{21} or R_{31} Fourier parameters. According to these authors, in the MCs their relations hold for F-mode pulsators with periods in

[5] This features can be explained taking into account that very young CCs can only be F pulsators, as youth implies higher mass and luminosity, and hence higher periods. We recall that the limiting periods for 1O pulsators is about 6 d.

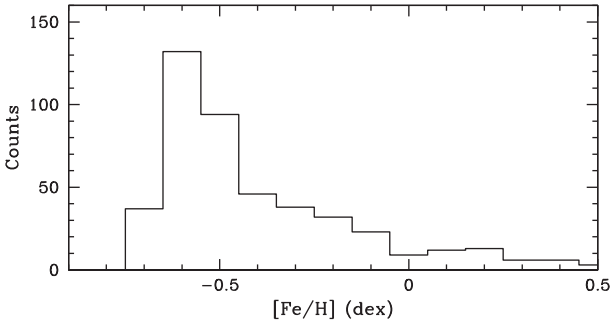

Figure 10. Distribution of the individual photometric metallicities for the CCs analysed in this work. Note that the absolute [Fe/H] values can be overestimated by ∼0.1 dex (see the text).

the range 2.5–4.0 d. To estimate the photometric [Fe/H] values, we thus adopted the Fourier parameters R_{31}[6] published by OGLE IV in the I band and transformed it in the V band, as according to Klagyivik et al. (2013), the I band is less sensitive to metallicity. The transformation used is the following:

$$R_{31}(V) = (0.005 \pm 0.008) + (0.96 \pm 0.05)R_{31}(I), \quad (3)$$

with an rms = 0.015 mag (Ripepi et al. in preparation). Finally, the relations showed in table 3 of Klagyivik et al. (2013) were used to calculate the [Fe/H] values for 462 CCs in the SMC. A histogram of the results is shown in Fig. 10. It can be seen that there is a peak at about [Fe/H] =−0.6 dex, with a tile of values reaching [Fe/H] =+0.5 dex (11 stars with [Fe/H] beyond this value are not shown). The minimum error on the individual photometric [Fe/H] values is given by the rms of the R_{31} versus [Fe/H] relationship adopted here, i.e. 0.082 mag. In addition, we have to consider the random errors on the OGLE IV R_{31} values, which are not available, and the uncertainty introduced by the use of equation (3). Moreover, the Klagyivik et al. (2013) relations have been calibrated with Galactic CCs which are more metal rich than SMC ones, so that our [Fe/H] values can be systematically overestimated by about 0.1 dex (see fig. 3 of Klagyivik et al. 2013). Overall, a conservative estimate of the total errors on the individual abundances is thus of the order of 0.2 dex. We note however that the contribution of random errors only should be smaller, so that relative individual abundances among the SMC should be more robust than absolute values. As for the stars with high values of [Fe/H] and in particular those with oversolar abundances, we are not fully confident about the reliability of these measures that can be affected by wrong values of R_{31}.

About 64 per cent and 73 per cent of the CCs have [Fe/H]<−0.4 and <−0.3 dex, respectively. The median of the distribution (to be preferred to the average, given the highly asymmetric distribution) of the whole sample is −0.50 ± 0.16 dex. This value become −0.56 ± 0.06 dex −0.52 ± 0.08 dex if we consider only pulsators with [Fe/H]<−0.4 and <−0.3 dex, respectively.

These values are somewhat higher than the estimate by Romaniello et al. (2008) [Fe/H] =−0.75 dex ($\sigma \sim 0.08$ dex) on the basis of a sample of 14 CCs observed with high-resolution spectroscopy, or that by Piatti & Geisler (2013), [Fe/H] =−0.70 dex ($\sigma \sim 0.15$ dex) based on Washington photometry of field stars (present-day metallicity, their fig. 6). The discrepancies are of the order of 0.2 and 0.15 dex for the whole and the more metal-poor samples, respectively. Hence, formally, our values agree with literatures' within $\sim 1\sigma$. However, as already remarked above, we expected to overestimate the abundances by some 0.1 dex due to the lack of metal-poor calibrators in Klagyivik et al. (2013)'s work, therefore the slight discrepancy observed is real.

[6] R_{31} is to be preferred to R_{21} for lower metallicities, see fig. 3 in Klagyivik et al. (2013).

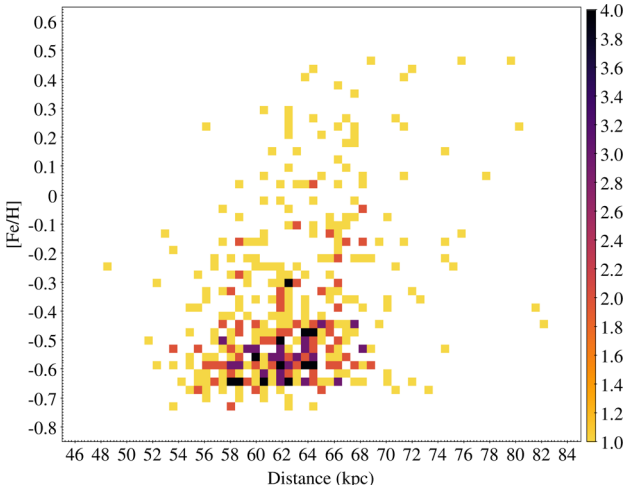

Figure 11. Photometric metallicities as a function of distance from the Sun. The centre of the SMC is placed at 63 kpc. The colour bar shows the number of objects in each bi-dimensional bin. Note that the high value of [Fe/H] measured for a minority of CCs can be affected by a large uncertainty (see the text).

In any case, it is reasonable to assume that the relative abundance differences are usable. Therefore, we searched for possible trends between metallicity and position in the SMC. Fig. 11 displays the photometric [Fe/H] values as a function of the distance from us. The figure shows that CCs closer than roughly 60 kpc seem preferentially more metal poor than objects between 60 and 70 kpc, i.e. roughly around the centre of SMC at 63 kpc. This could imply that the stripped material from which the more external CCs formed was relatively metal poor, while the one closest to the centre was enriched between the time when there was a tidal interaction that brought out the material and the time when the Cepheids were formed. However, we remind our warning about the possible large uncertainties affecting high abundance evaluations. Indeed, considering the sample of objects with [Fe/H]<−0.4 dex, the distribution appears rather uniform with distance.

4.3 Distribution of CCs on the sky

We divided our sample of CCs according to their distances, adopting an interval of 2.5 kpc between adjacent subsamples. This value was chosen because it is larger than the individual errors on the distances. It is also sufficiently small to allow us to investigate in detail the distribution of CCs in the sky including a statistically significant number of stars in each interval. The result of this exercise is shown in Fig. 12 where we show the distribution of the CCs in the sky (following van der Marel & Cioni 2001, we adopted a Cartesian zenithal equidistant projection) at varying distances and different colours for ages < 140 Myr (blue) and ≥ 140 Myr (red). The relative distances shown in the figure have been obtained with the $PW(V, K_s)$, but we verified that the use of the $PW(J, K_s)$ leads to the same results.

An analysis of the figure confirms that the SMC is highly elongated along the LOS. However, the exquisite accuracy of our relative distance determinations allows us to detect more details about the

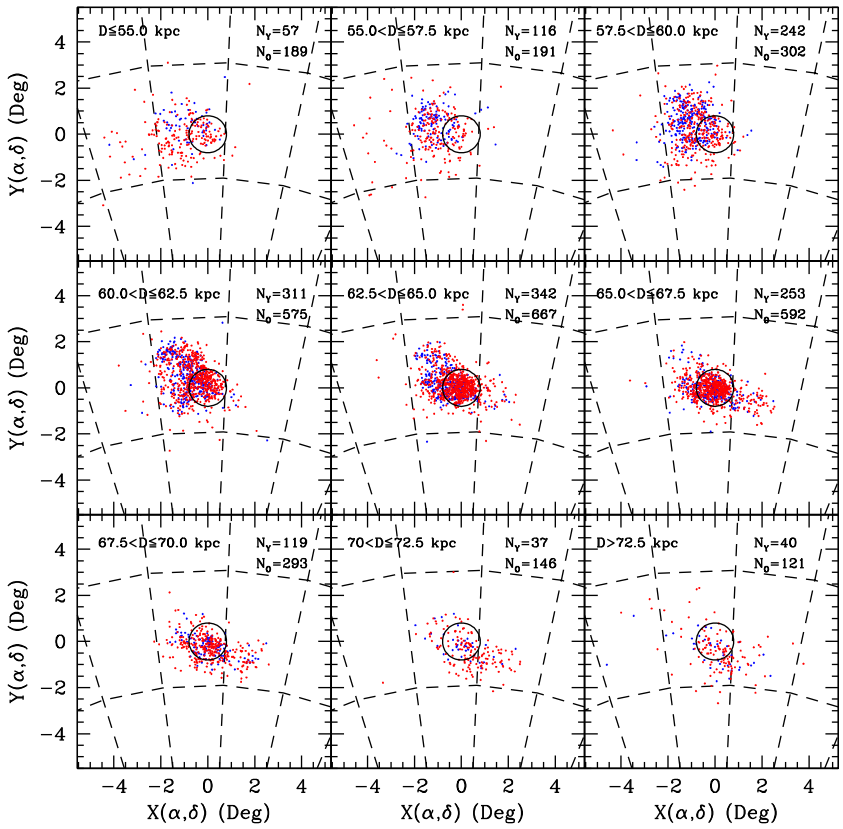

Figure 12. Distribution of SMC CCs on the sky at varying distances. Blue and red dots show pulsators with age < 140 Myr and age ≥ 140 Myr, respectively. The number of pulsators within or beyond this threshold are labelled in each panel with $N_{\rm Y}$ and $N_{\rm O}$, respectively. A circle centred on (0,0) coordinates and with radius = 0.8 kpc has been drawn in each panel for reference. Note that in this zenithal equidistant projection, N is up and E is to the left (the X-axis is antiparallel to the α axis). The centre is at $\alpha_0 = 12.54$ deg; $\delta_0 = -73.11$ deg.

structure of the galaxy. First, using the central circle with radius = 0.8 kpc as reference, it can be easily seen that the galaxy is elongated roughly from east (E) towards the west/south-west (W/SW) direction, with the stars in the latter position the farthest from us. The structure of the SMC appears approximately round closer to us (for distances smaller than ∼60 kpc) and becomes progressively asymmetric going to greater distances, assuming an asymmetric distribution with inclination in the north-west (NW)–south-east (SE) direction, that can be clearly seen beyond ∼ 65 kpc. Around the distance of the centre of the galaxy, i.e. 63 kpc, there is a bulk of CCs with approximately round shape (and radius of about 0.8 kpc, as shown by the circle in the figure) that is visible until 67.5 kpc. A strong structure is present in the NE direction between 57.5 and 65 kpc (similar to the northern structure discussed by Jacyszyn-Dobrzeniecka et al. 2016). At 65 kpc this NE structure disappears and a concentration of stars in the SW direction becomes visible. This feature is present until and beyond 72.5 kpc. There are apparently no clear trends with the age of the pulsators, apart from a striking feature present for distances smaller than 55 kpc (uppermost-left panel in Fig. 12) in the easternmost part of the whole galaxy distribution. The pulsators in this isolated region are predominantly older than 140 Myr. We will speculate further on the age trends in the next section.

4.4 Distribution of CCs in 3D Cartesian space

The distribution of SMC CCs in Cartesian 3D space is shown in Fig. 13, where the left-hand and right-hand panels show the sample of CCs with age ≥140 Myr and age < 140 Myr, respectively. The scales along the three axes are the same, so that the elongated nature of the distribution of CCs in the SMC can be easily seen. As already noted by Jacyszyn-Dobrzeniecka et al. (2016) and Scowcroft et al. (2016), the distribution of CCs in the SMC is not planar, but rather ellipsoidal, irregular and somewhat fragmented. Some of them are more evident in the old sample (age $\geq$ 140 Myr), whereas others stand out clearly in the young sample (age < 140 Myr). These features can be discussed more in detail by analysing the projection in the Cartesian X, Y plane for different values of Z, as shown in Figs 14 and 15 for the old and young samples, respectively. An analysis of these figures reveals a close similarity with Fig. 12, indicating that the elongation of the SMC is almost along the LOS. The presence of an off-centre eastern structure for Z of less than approximately 60 kpc is confirmed. This structure is almost completely populated by CCs of the old sample, which also shows an extreme E/SE component, almost absent from the young sample. Beyond 60 kpc the general distribution of CCs is more centred, and the most evident substructure is shifted towards the NW. Between 60.0 and 62.5 kpc, this north-eastern substructure is more evident in the young sample, which seems to show a possible trimodal distribution in this interval of distance. Looking at Fig. 13 (right-hand panel) and Fig. 15 (mid-leftmost panel), the possible centres of this trimodal distribution are located approximately around (−0.5,0.0), (−1.0, −1.0) and (−1.5, −2) kpc, respectively. Some signs of this feature are present until $Z \sim 65.0$ kpc in the young sample, whereas the old one is almost clustered in the central 1 kpc. Beyond $Z = 65.0$ kpc the young sample is almost centred without significant substructures.

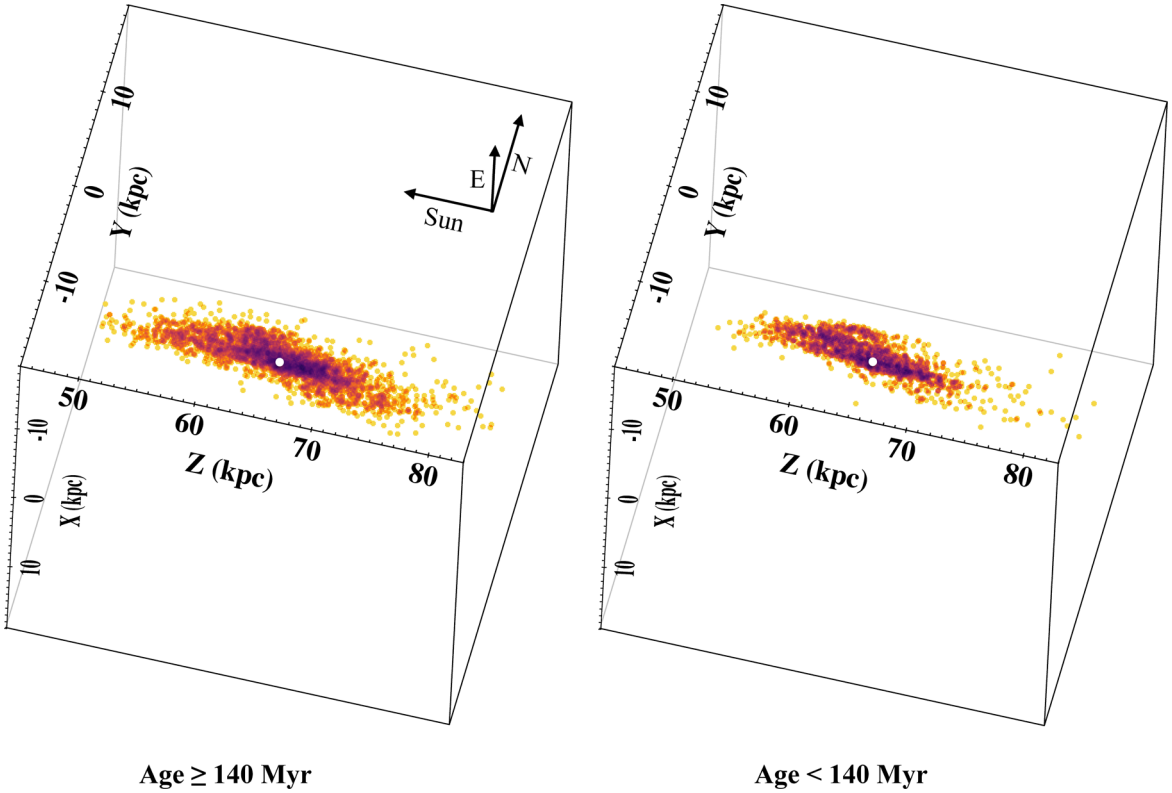

Figure 13. Three-dimensional Cartesian distribution of the SMC CCs for the labelled ages. The colour scale is proportional to the star density. In both panels, a white filled circle shows the approximate centroid of the whole sample of CCs adopted in this work ($\alpha_0 = 12.54$ deg; $\delta_0 = -73.11$ deg).

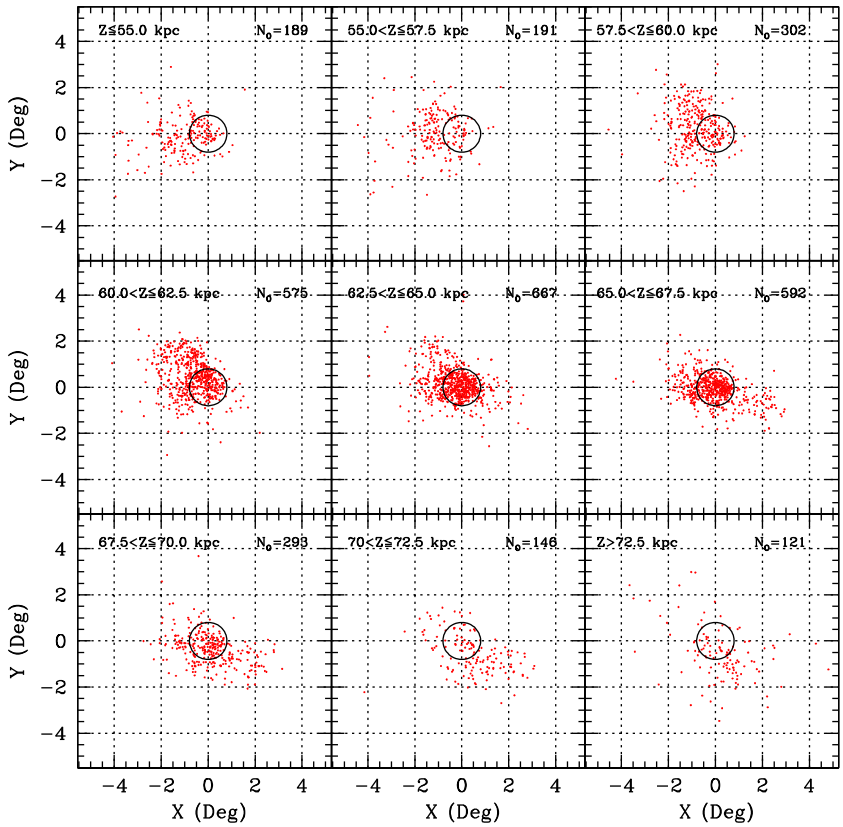

Figure 14. Cartesian *X*, *Y* plane at varying *Z* for the old sample (age ≥ 140 Myr). As in Fig. 12, each panel shows a circle centred on (0,0) coordinates and with radius = 0.8 kpc.

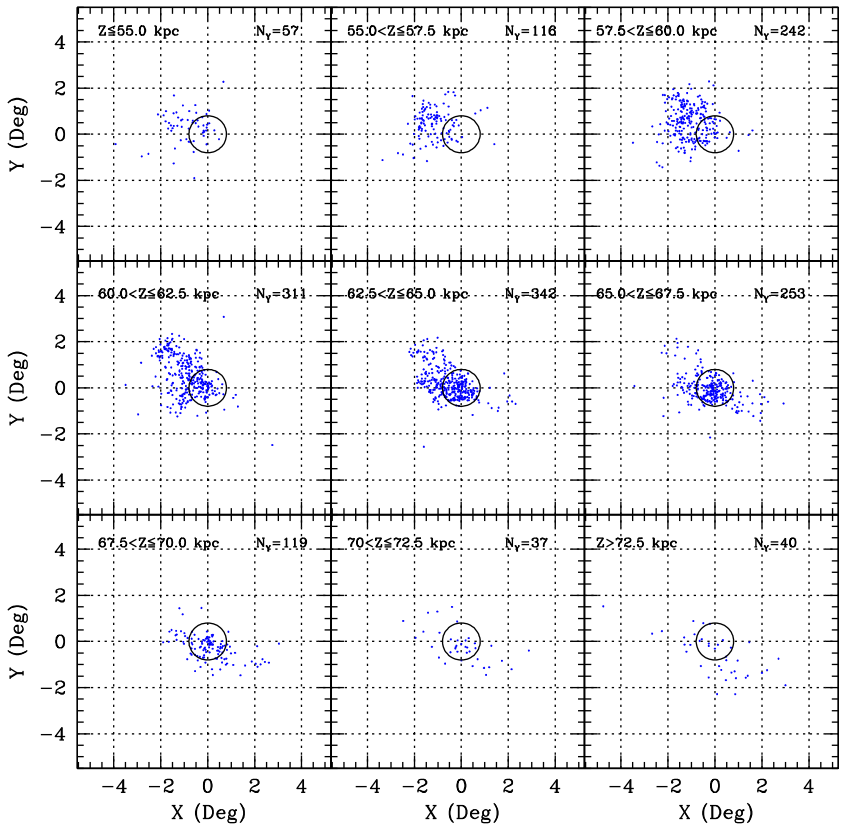

Figure 15. As in Fig. 14 for the young sample (age < 140 Myr).

On the contrary, the old sample shows a remarkable SW structure extending from $Z \sim 65.0$ kpc to $Z \sim 72.5$ kpc and beyond (see also Jacyszyn-Dobrzeniecka et al. 2016). Summarizing, the old sample appears to be more elongated than the young one both in the E (closer to us) and in the SW (farther from us) directions (this is in contrast with Jacyszyn-Dobrzeniecka et al. 2016, who found that the stars closer to us are also the youngest). The young sample is thus more compact than the old one, as there are very few young CCs closer than 55 kpc and beyond $Z \sim 70$ kpc. Its location is apparently on average more off-centre (see Figs 14 and 15 for Z between 60 and 67.5 kpc) with respect to the bulk of old CCs. Taking into account that the LMC is located in the E/NE (depending on the distance) direction with respect to the SMC, we can use this empirical evidence to suggest a tentative explanation for this complex distribution. Thus, the population to which the old CCs belong underwent a strong interaction with the LMC when they had already been formed (i.e. >140 Myr ago) and the signatures of this event are (i) the distribution of stars closer than ∼60 kpc heavily off-centred in the E/NE direction, i.e. towards the LMC; (ii) the spread of old pulsators in the opposite direction (SW), as expected in case of strong tidal interactions (see also Section 5). On the contrary, the young CCs were probably formed after that event, but part of the gas/material from which they formed was already subject to this gravitational interaction. This would explain the strong off-centred (eastern) position of the majority of the young CCs until $Z \sim 60$ kpc, and the NE substructure(s) clearly visible among young pulsators for Z between ∼60 and ∼65 kpc. In this scenario, the lack of young pulsators for $Z > 70$ kpc can be explained by hypothesizing that the gas/material tidally stripped in this direction, if any, did not possess sufficient density to trigger strong star formation, because originally more concentrated in the SMC's body (in this region there is no strong recent star formation, see e.g. Rubele et al. 2015).

This scenario can be further appreciated by plotting the CC distribution in terms of Galactic longitude versus distance, see Fig. 16. In addition, to show a more complete picture of the MS, we plotted the positions of the ab-type RR Lyrae stars in the same plane for both the LMC (green dots) and SMC (cyan dots). The distances of the RR Lyrae variables in both galaxies were derived from the optical OGLE IV photometry as explained in Appendix B. The figure also shows with black arrows the direction of motion of the two galaxies (i.e. the position they will reach in 50 Myr), according to the proper motion measurements of van der Marel & Sahlmann (2016). This figure suggests that (i) in the SMC, the distributions of the CCs and RR Lyrae have the same elongation, but different shapes, in the sense that the RR Lyrae stars define a larger spheroidal or ellipsoidal volume (see Jacyszyn-Dobrzeniecka et al. 2017; Muraveva et al. 2017, and references therein); (ii) it is confirmed that the distribution of the young CCs is more compact than the old CCs one; (iii) the elongation of the SMC is approximately oriented in the direction of the MW, but there are clear hints of a distortion, visible especially for old pulsators in the direction of the LMC in the distance range from 50 to 60 kpc; (iv) the elongation of the SMC CCs is consistent with the direction of the SMC motion.

5 DISCUSSION

Previous results on the three-dimensional structure of SMC CCs, obtained by Haschke et al. (2012) and Subramanian & Subramaniam (2015), based on OGLE III data, were based on the assumption that the young stars are more likely to have a disc distribution. This

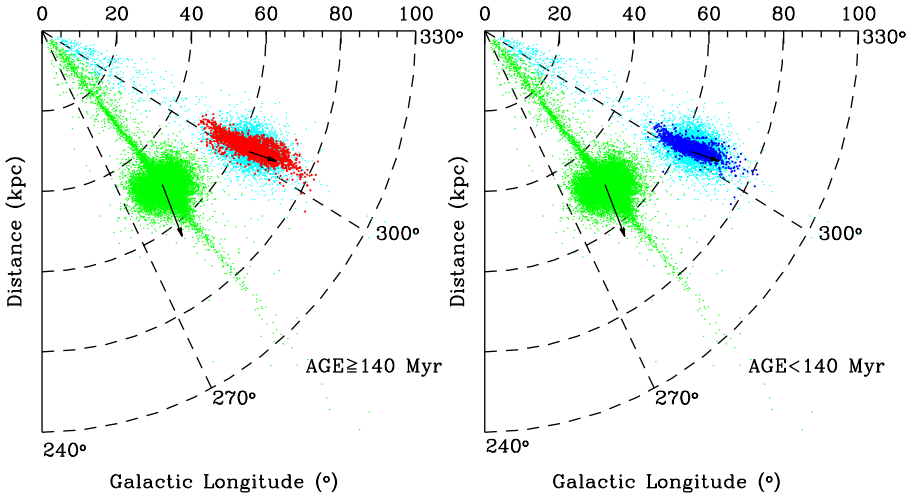

Figure 16. Polar projection of Galactic longitude coordinates for the old (red dots) and young (blue dots) CC samples in the SMC. For comparison, the ab-type RR Lyrae stars in the SMC (cyan dots) and in the LMC (green dots) are shown. The black arrows show the directions of motion of the two galaxies (the position they will reach in 50 Myr), according to the proper motion measurements of van der Marel & Sahlmann (2016). We note that according to Jacyszyn-Dobrzeniecka et al. (2017), the straight lines of stars connecting between $R = 0$ kpc to $R = 80$ kpc in both the LMC and SMC are either true Galactic RR Lyrae variables along the LOS or (in large majority) pulsators whose distances are strongly affected by blending/crowding or other photometric errors.

assumption was based on the spectroscopic study of young stars by Evans & Howarth (2008) and Dobbie et al. (2014). The latter authors suggested that the red giant distribution in the SMC is better explained by a rotating disc of inclination and position angle of the line of nodes similar to that of the parameters of the disc found using CCs. These results were contradicted by the recent work of van der Marel & Sahlmann (2016), who used *HST* and *Gaia* proper motions in the SMC, finding no significant rotation (i.e. the signature of a distribution on a disc) for young stars, as that seen in previous studies (but van der Marel & Sahlmann 2016, state that the next data release of *Gaia* is needed to obtain conclusive results). In any case, in the disc model by Haschke et al. (2012) and Subramanian & Subramaniam (2015) the large elongation along LOS is explained as due to a large inclination of the disc.

However, these outcomes were questioned by recent works based on more accurate measurements (Scowcroft et al. 2016), or more extended samples (Jacyszyn-Dobrzeniecka et al. 2016) of CCs. Our results, as presented in the previous section are in substantial agreement with these two latter works. Indeed, we support their conclusions concerning (i) the SMC CC distribution is not planar, but elongated approximating an ellipsoidal shape with significant substructures; (ii) a different distribution of the young and old CC samples (Jacyszyn-Dobrzeniecka et al. 2016) and the rotation of the distribution in the direction of the LMC (Scowcroft et al. 2016). However, the high precision of our measurements exploiting the NIR bands allowed us to carry out the finest characterization of the three-dimensional distribution of SMC CCs.

Very recently Subramanian et al. (2017), using VMC survey data for intermediate-age RC stars, found a foreground population at about 12 ± 2 kpc (with respect to the SMC centre) from the inner ($r \sim 2°$) to the outer ($r \sim 4°$) regions in the eastern SMC. They propose that these stars have been tidally stripped from the SMC during the most recent LMC–SMC encounter and thus offer evidence of the tidal origin of the MB. An inspection of Figs 13–16 reveals that our results do not support such a bimodal distribution of CCs in the eastern regions of the SMC, even for the old CC population, which is expected to be affected by the close encounter with the LMC (the younger one should have formed CCs after that episode) as for the intermediate-age RC stars. However, we have only a few CCs at radii larger than 2 deg in the eastern direction (see the top-leftmost panel of Fig. 12), where, according to Subramanian et al. (2017), the effect of the bimodality of RC stars is maximum. Moreover, these easternmost CCs are at closer distances to us than the SMC centroid (>8 kpc closer). On the basis of these considerations, we can conclude that the results from CCs and RC are consistent.

The results presented in the previous section can also be compared with the predictions of Diaz & Bekki (2012). To this end we constructed a figure similar to their fig. 8, but using our data for RR Lyrae stars in the LMC and SMC, as well as for young and old CCs in the SMC. The result of this exercise is shown in Fig. 17, where, following Diaz & Bekki (2012), we adopted the Magellanic Coordinate System ($L_{\rm MS}$, $B_{\rm MS}$) introduced by Nidever, Majewski & Butler Burton (2008). It is worth recalling that one of the most prominent features in Diaz & Bekki (2012)'s predictions, is the existence of the CB in opposite direction with respect to the MB. The presence of CB in the western region was also discussed briefly in Subramanian & Subramaniam (2015). There the CB counter-parts are identified as those which are out of the plane and behind the disc, i.e. CCs at distances of 70–80 kpc. In Fig. 17, the CB is expected to be located at $(L_{\rm MS}, B_{\rm MS}) \approx (-16°, -6°)$ in the bottom-left panel of Fig. 17, between $-4° \lesssim B_{\rm MS} \lesssim -16°$ in the top-left panel and $-14° \lesssim L_{\rm MS} \lesssim -20°$ in the bottom-right panel. These locations have been approximately highlighted in the figure to make the comparison with Diaz & Bekki (2012)'s fig. 8 easier. An inspection of Fig. 17, thus reveals that the regions where the CB is expected are partially populated (both in $B_{\rm MS}$ versus distance and $L_{\rm MS}$ versus distance diagrams) by old CCs as well as RR Lyrae, whereas young CCs are more centrally concentrated. This finding is in agreement with our scenario outlined in Section 4.4 and seems to confirm Diaz & Bekki (2012)'s model predictions.

Fig. 17 shows additional interesting features showing once again the effects of the interaction between the MCs: (i) the already known fact that there is no actual separation between the two MCs is clearly visible in these plots; (ii) the distribution of RR Lyrae and CCs is clearly disturbed by the presence of the LMC; (iii) the distribution of young CCs is different from that of the old ones,

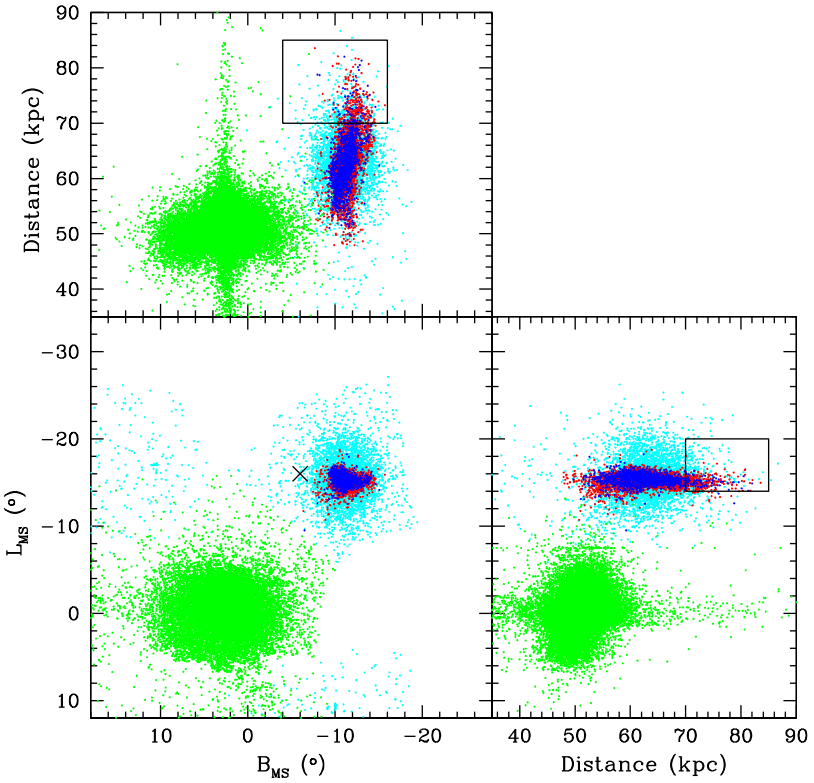

Figure 17. Position of LMC and SMC RR Lyrae as well as of young and old CCs in the SMC (same colour coding as in Fig 16) in Magellanic coordinates (bottom-left) or Magellanic longitude/latitude versus distance (bottom-right and top-left, respectively). This figure is similar to fig. 8 of Diaz & Bekki (2012), whose prediction can be directly compared. The approximate location of the predicted Counter-Bridge are shown with a diagonal cross (centre) in the bottom-left panel and with boxes in the top-left and bottom-right panels. The colour code of the data points is the same as in Fig. 16.

being more concentrated and showing a larger rotation towards the LMC, especially in the B_{MS} versus distance plane.

These features are also in fair agreement with Model 2 of Besla et al. (2012), based on the hypothesis of a direct collision between the MCs, leaving a trail of stars between the MCs. This presence is evidenced by the continuous distribution of pulsators in Fig. 17 (as well as in Fig. 16). Besla et al. (2012)'s model also predicts star formation along the MB at an epoch compatible with the age of the CCs (e.g. 100–300 Myr). From our analysis, the CCs closer to the MB appear to be the oldest ones but this does not appear in contrast with this model, given the wide range of ages encompassed by Besla et al. (2012)'s prediction.

6 CONCLUSIONS

In this paper, we have presented the VMC survey's light curves for 717 CCs in the SMC. These data complete and complement our previous Paper I, resulting in a sample of 4793 CCs in SMC for which we provide here Y, J and K_s average magnitudes, amplitudes and relative errors, calculated as in Paper I. Our work represents the complement to the optical study of CCs in the SMC carried out by the OGLE group (Soszyński et al. 2015b; Jacyszyn-Dobrzeniecka et al. 2016).

The intensity-averaged magnitudes in the VISTA Y, J and K_s filters have been complemented with optical V-band data and periods to construct multifilter PL and PW relations for SMC CCs. In particular, the PL and PW relations in the V, J and K_s bands for F- and 1O-mode SMC CCs presented in this work are the most accurate to date, based on well- or moderately well-sampled light curves in K_s and J, respectively.

We used these relations to estimate accurate individual CC distances in the SMC covering an area of more than 40 deg^2. Adopting literature relations, we estimated ages and metallicities for the majority of the investigated pulsators, finding that (i) the age distribution is bimodal, with two peaks at 120 and 220 Myr and a break at 140 Myr; (ii) the more metal-rich CCs appear to be located closer to the centre of the galaxy.

We provided the most accurate 3D distribution of the CCs in the SMC to date. We conclude that, in agreement with the literature, the distribution of the CCs is not planar but significantly elongated over more than 25–30 kpc approximately in the E/NE towards SW direction. Our exquisite photometry allowed us to describe in great detail the substructures present in the SMC. In more detail, the young and old CC populations in the SMC seem to show different distributions. The distribution of the old CCs is more elongated with respect to the young one that is more centrally concentrated. Both old and young stars show strong off–centre structures due to the history of interaction with the LMC.

A possible scenario able to explain the present time 3D geometry of the CCs in the SMC is the following: the population, to which the old CCs belong, underwent a strong interaction with the LMC when they were already formed (i.e. >140 Myr ago). The signatures of this event are (i) the distribution of stars closer than ∼60 kpc heavily off-centred in the E/NE direction, i.e. towards the LMC; (ii) the spread of old pulsators in the opposite direction (SW), as expected for strong tidal interactions. On the contrary, the young CCs were probably formed after that event, but part of the gas/material

from which they formed was already subject to gravitational interaction. This would explain the strong off-centre (eastern) position of the majority of the young CCs until $Z \sim 60$ kpc, and the NE substructure(s) clearly visible among young pulsators for Z between $\sim$60 and $\sim$65 kpc. In this scenario, the lack of young pulsators at $Z > 70$ kpc can be explained by hypothesizing that the gas/material tidally stripped in this direction did not have sufficient density to trigger strong star formation (in this region there is no strong recent star formation, see e.g. Rubele et al. 2015).

In addition, our results indicate that the shape of the SMC is elongated and somewhat rotated towards the LMC in the region closer to this galaxy, as expected from the hypothesis of a direct collision or a close encounter some 200 Myr ago.

A detailed comparison between our observations and the Diaz & Bekki (2012) predictions showed a fairly good overall agreement, with the first confirmation of the presence of the CB, remaining after the last close LMC–SMC encounter. It appears now clear that a new generation of models of the MS is needed to explain the detailed and complex structure of the young SMC component traced by its CC population, and described in detail in this paper.

Finally, we do not think that much progress in the knowledge of the geometry of the SMC will be possible in the future from the photometry of CC variables only. Though, information is lacking about proper motions, radial velocities and abundances for these stars. Proper motions will be the subject of future works in the context of the VMC survey itself (see e.g. Cioni et al. 2016) or available for not too crowded objects by means of the *Gaia* satellite measurements. Massive spectroscopic surveys of the pulsating variables will be possible within a few years thanks to instruments such as 4MOST@VISTA and MOONS@VLT. The sum of this complementary information will eventually allow us to unveil with great confidence the 'true' story of the formation and evolution of the SMC and MS as a whole.

ACKNOWLEDGEMENTS

We thank D.L. Nidever for kindly providing us with the code to transform Galactic to Magellanic coordinates.

This paper is based on observations obtained with the ESO/VISTA telescope located at Paranal (Chile). We thank the UK's VISTA Data Flow System comprising the VISTA pipeline at CASU and the VISTA Science Archive at Wide Field Astronomy Unit (Edinburgh; WFAU) for providing calibrated data products supported by the STFC.

This project has received funding from the European Research Council (ERC) under the European Union's Horizon 2020 research and innovation programme (grant agreement No. 682115). MRLC acknowledges support from the UK's Science and Technology Facility Council (grant number ST/M001008/1).

RdG is grateful for research support from the National Natural Science Foundation of China through grants U1631102, 11373010 and 11633005.

SS acknowledges research funding support from the Chinese Postdoctoral Science Foundation (grant number 2016M590013).

REFERENCES

Anderson R. I., Saio H., Ekström S., Georgy C., Meynet G., 2016, A&A, 591, A8
Bekki K., Chiba M., 2008, ApJ, 679, L89
Belokurov V., Erkal D., Deason A. J., Koposov S. E., De Angeli F., Evans D. W., Fraternali F., Mackey D., 2017, MNRAS, 466, 4711
Besla G., Kallivayalil N., Hernquist L., Robertson B., Cox T. J., van der Marel R. P., Alcock C., 2007, ApJ, 668, 949
Besla G., Kallivayalil N., Hernquist L., van der Marel R. P., Cox T. J., Kereš D., 2012, MNRAS, 421, 2109
Bono G., Caputo F., Castellani V., Marconi M., 1999, ApJ, 512, 711
Bono G., Marconi M., Cassisi S., Caputo F., Gieren W., Pietrzynski G., 2005, ApJ, 621, 966
Bono G., Caputo F., Marconi M., Musella I., 2010, ApJ, 715, 277
Caldwell J. A. R., Coulson I. M., 1986, MNRAS, 218, 223
Caputo F., Marconi M., Musella I., 2000, A&A, 354, 610
Cardelli J. A., Clayton G. C., Mathis J. S., 1989, ApJ, 345, 245
Cioni M.-R. L., Habing H. J., Israel F. P., 2000, A&A, 358, L9
Cioni M.-R. L. et al., 2011, A&A, 527, 116
Cioni M.-R. L. et al., 2016, A&A, 586, A77
Cross N. J. G. et al., 2012, A&A, 548, A119
D'Onghia E., Fox A. J., 2016, ARA&A, 54, 363
de Grijs R., Bono G., 2015, AJ, 149, 179
de Grijs R., Wicker J. E., Bono G., 2014, AJ, 147, 122
Deason A. J., Wetzel A. R., Garrison-Kimmel S., Belokurov V., 2015, MNRAS, 453, 3568
Deb S., Singh H. P., Kumar S., Kanbur S. M., 2015, MNRAS, 449, 2768
Diaz J. D., Bekki K., 2012, ApJ, 750, 36
Dobbie P. D., Cole A. A., Subramaniam A., Keller S., 2014, MNRAS, 442, 1663
Drlica-Wagner A. et al., 2015, ApJ, 813, 109
Drlica-Wagner A. et al., 2016, ApJ, 833, L5
Emerson J. P. et al., 2004, in Quinn P. J., Bridger A., eds, Proc. SPIE Conf. Ser. Vol. 5493, Optimizing Scientific Return for Astronomy through Information Technologies. SPIE, Bellingham, p. 401
Evans C. J., Howarth I. D., 2008, MNRAS, 386, 826
Gaia Collaboration, 2016a, A&A, 595, A1
Gaia Collaboration, 2016b, A&A, 595, A2
Gao J., Jiang B. W., Li A., Xue M. Y., 2013, ApJ, 776, 7
Gardiner L. T., Noguchi M., 1996, MNRAS, 278, 191
Glatt K. et al., 2008, AJ, 136, 1703
Gonidakis I., Livanou E., Kontizas E., Klein U., Kontizas M., Belcheva M., Tsalmantza P., Karampelas A., 2009, A&A, 496, 375
González-Fernández C. et al., 2017, A&A, in press
Hammer F., Yang Y. B., Flores H., Puech M., Fouquet S., 2015, ApJ, 813, 110
Harris, 2007, ApJ, 658, 345
Harris J., Zaritsky D., 2004, AJ, 127, 1531
Harris J., Zaritsky D., 2006, AJ, 131, 2514
Harris J., Zaritsky D., 2009, AJ, 138, 1243
Haschke R., Grebel E. K., Duffau S., 2011, AJ, 141, 158
Haschke R., Grebel E. K., Duffau S., 2012, AJ, 144, 107
Hatzidimitriou D., Hawkins M. R. S., 1989, MNRAS, 241, 667
Inno L. et al., 2016, ApJ, 832, 176
Irwin M. J., Kunkel W. E., Demers S., 1985, Nature, 318, 160
Irwin M. J. et al., 2004, in Quinn P. J., Bridger A., eds, Proc. SPIE Conf. Ser. Vol. 5493, Optimizing Scientific Return for Astronomy through Information Technologies. SPIE, Bellingham, p. 411
Jacyszyn-Dobrzeniecka A. M. et al., 2016, Acta Astron., 66, 149
Jacyszyn-Dobrzeniecka A. M. et al., 2017, Acta Astron., 67, 1
Jethwa P., Erkal D., Belokurov V., 2016, MNRAS, 461, 2212
Jurcsik J., Kovacs G., 1996, A&A, 312, 111
Kallivayalil N., van der Marel R. P., Besla G., Anderson J., Alcock C., 2013, ApJ, 764, 161
Kerber L. O., Girardi L., Rubele S., Cioni M.-R., 2009, A&A, 499, 697
Klagyivik P., Szabados L., Szing A., Leccia S., Mowlavi N., 2013, MNRAS, 434, 2418
Koposov S. E., Belokurov V., Torrealba G., Evans N. W., 2015, ApJ, 805, 130
Mackey A. D., Koposov S. E., Erkal D., Belokurov V., Da Costa G. S., Gómez F. A., 2016, MNRAS, 459, 239
Maragoudaki F., Kontizas M., Morgan D. H., Kontizas E., Dapergolas A., Livanou E., 2001, A&A, 379, 864

Marconi M., Bono G., Caputo F., Cassisi S., Pietrukowicz P., Pietrzynski G., Gieren W., 2006, Mem. Soc. Astron. Ital., 77, 67
Marconi M. et al., 2015, ApJ, 808, 50
Marconi M. et al., 2017, MNRAS, 466, 3206
Martin N. F. et al., 2016, ApJ, 830, L10
Moretti M. I. et al., 2014, MNRAS, 437, 2702
Moretti M. I. et al., 2016, MNRAS, 459, 1687
Muraveva T. et al., 2014, MNRAS, 443, 432
Muraveva T. et al., 2015, ApJ, 807, 127
Muraveva T. et al., 2017, MNRAS, submitted
Nemec J. M. et al., 2011, MNRAS, 417, 1022
Nemec J. M., Cohen J. G., Ripepi V., Derekas A., Moskalik P., Sesar B., Chadid M., Bruntt H., 2013, ApJ, 773, 181
Nidever D. L., Majewski S. R., Butler Burton W., 2008, ApJ, 679, 432
Nidever D. L., Monachesi A., Bell E. F., Majewski S. R., Muñoz R. R., Beaton R. L., 2013, ApJ, 779, 145
Noël N. E. D., Conn B. C., Read J. I., Carrera R., Dolphin A., Rix H.-W., 2015, MNRAS, 452, 4222
Piatti A. E., Geisler D., 2013, AJ, 145, 17
Pieres A. et al., 2017, MNRAS, 468, 1349
Putman M. E. et al., 1998, Nature, 394, 752
Ripepi V., Moretti M. I., Clementini G., Marconi M., Cioni M. R., Marquette J. B., Tisserand P., 2012a, Ap&SS, 341, 51
Ripepi V. et al., 2012b, MNRAS, 424, 1807
Ripepi V. et al., 2014a, MNRAS, 437, 2307
Ripepi V. et al., 2014b, MNRAS, 442, 1897
Ripepi V. et al., 2015, MNRAS, 446, 3034
Ripepi V. et al., 2016, ApJS, 224, 21 (Paper I)
Romaniello M. et al., 2008, A&A, 488, 731
Rubele S. et al., 2015, MNRAS, 449, 639
Sales L. V., Navarro J. F., Kallivayalil N., Frenk C. S., 2017, MNRAS, 465, 1879
Scowcroft V., Freedman W. L., Madore B. F., Monson A., Persson S. E., Rich J., Seibert M., Rigby J. R., 2016, ApJ, 816, 49
Shapley H., 1940, Harvard College Obs. Bull., 914, 8
Soszyński I. et al., 2010, Acta Astron., 60, 17
Soszyński I. et al., 2015a, Acta Astron., 65, 297
Soszyński I. et al., 2015b, Acta Astron., 65, 329
Soszyński I. et al., 2016, Acta Astron., 66, 131
Stanimirović S., Staveley-Smith L., Jones P. A., 2004, ApJ, 604, 176
Subramanian S., Subramaniam A., 2012, ApJ, 744, 128
Subramanian S., Subramaniam A., 2015, A&A, 573, A135
Subramanian S. et al., 2017, MNRAS, 467, 2980
Tisserand P. et al., 2007, A&A, 469, 387
Udalski A., Szymański M. K., Szymański G., 2015a, Acta Astron., 65, 1
Udalski A. et al., 2015b, Acta Astron., 65, 341
van der Marel R. P., Cioni M.-R. L., 2001, AJ, 122, 1807
van der Marel R. P., Sahlmann J., 2016, ApJ, 832, L23
Weinberg M. D., Nikolaev S., 2001, ApJ, 548, 712
Welch D. L., McLaren R. A., Madore B. F., McAlary C. W., 1987, ApJ, 321, 162
Yoshizawa A. M., Noguchi M., 2003, MNRAS, 339, 1135
Zaritsky D., Harris J., Grebel E. K., Thompson I. B., 2000, ApJ, 534, L53

SUPPORTING INFORMATION

Supplementary data are available at *MNRAS* online.

online materil.tar.gip

Please note: Oxford University Press is not responsible for the content or functionality of any supporting materials supplied by the authors. Any queries (other than missing material) should be directed to the corresponding author for the article.

APPENDIX A: LIGHT CURVES

The VMC light curves in Y, J and K_s filters of the 717 CCs analysed in this paper and not present in Paper I are shown in Figs A1, A2 and A3, respectively. The figures also include the 40 stars already present in Paper I but for which the number of epochs has been almost doubled.

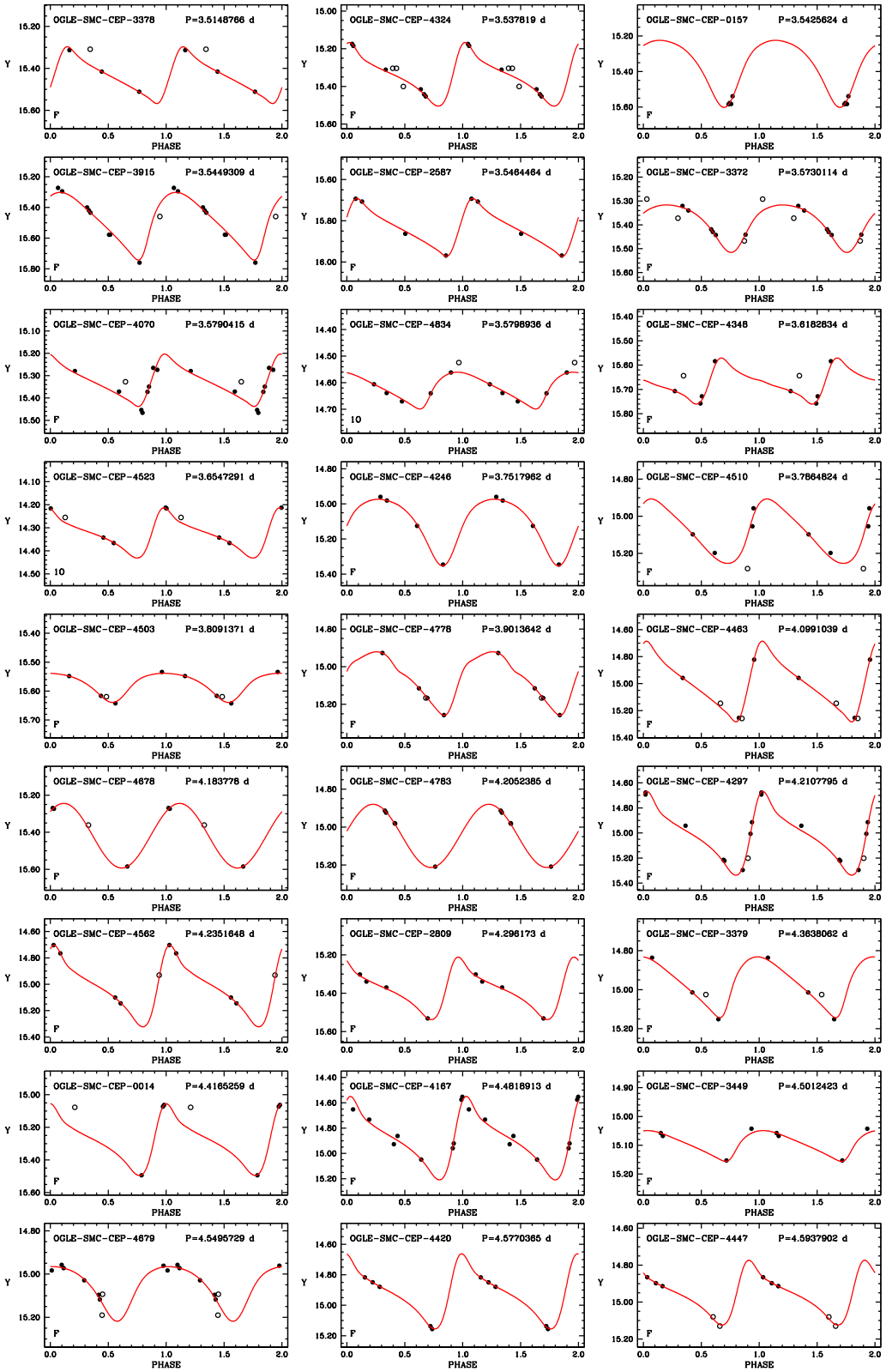

Figure A1. *Y*-band light curves for the 757 CCs with new data with respect to Paper I (see the text). Stars are displayed in order of increasing period. Filled and open circles represent phase points used or not used in the fitting procedure, respectively (see Paper I). Solid lines represent best-fitting templates to the data (see the text). In each panel, we report OGLE's identification number, mode of pulsation and period.

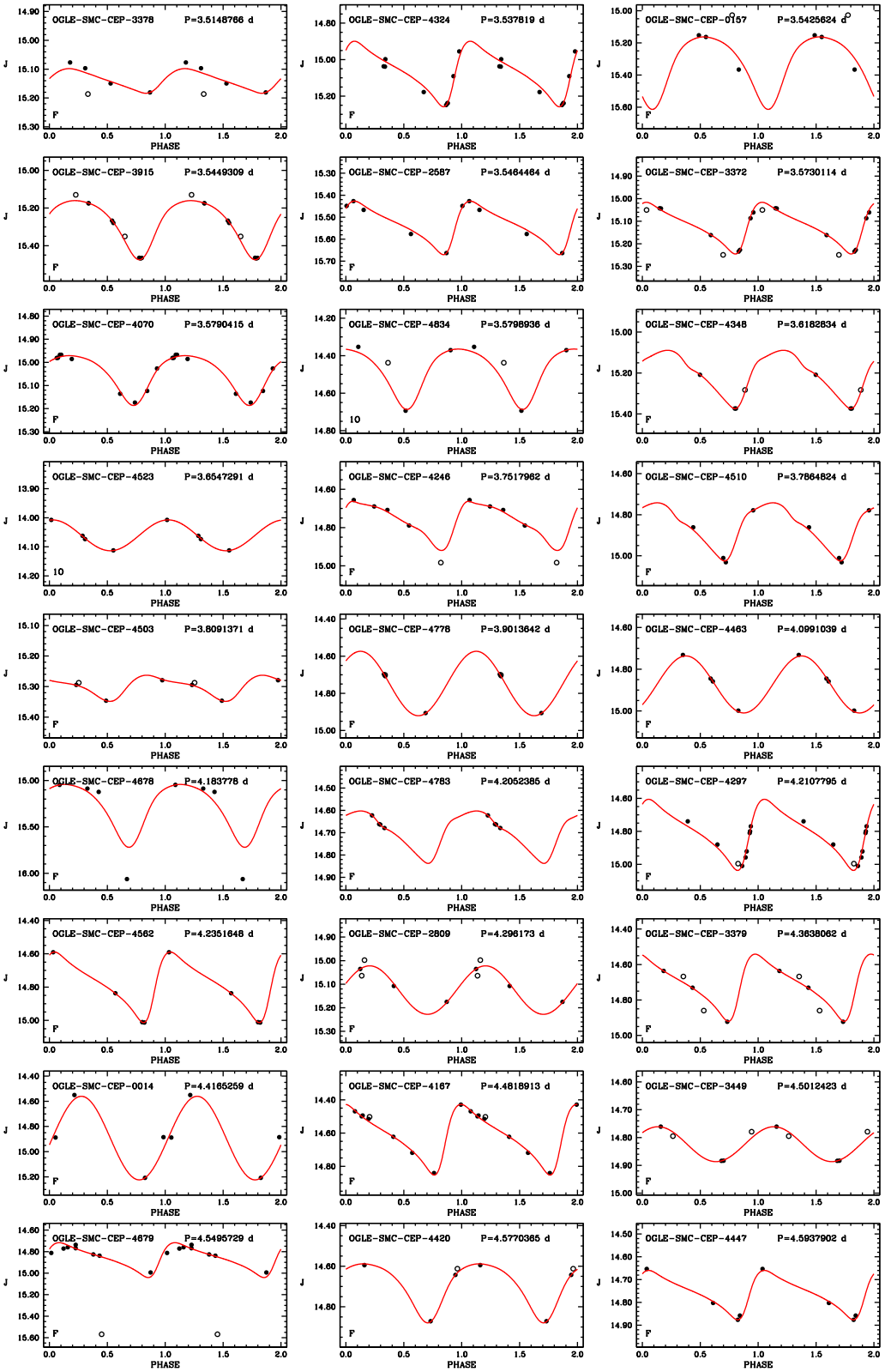

Figure A2. Same as in Fig. A1 but for the *J* band.

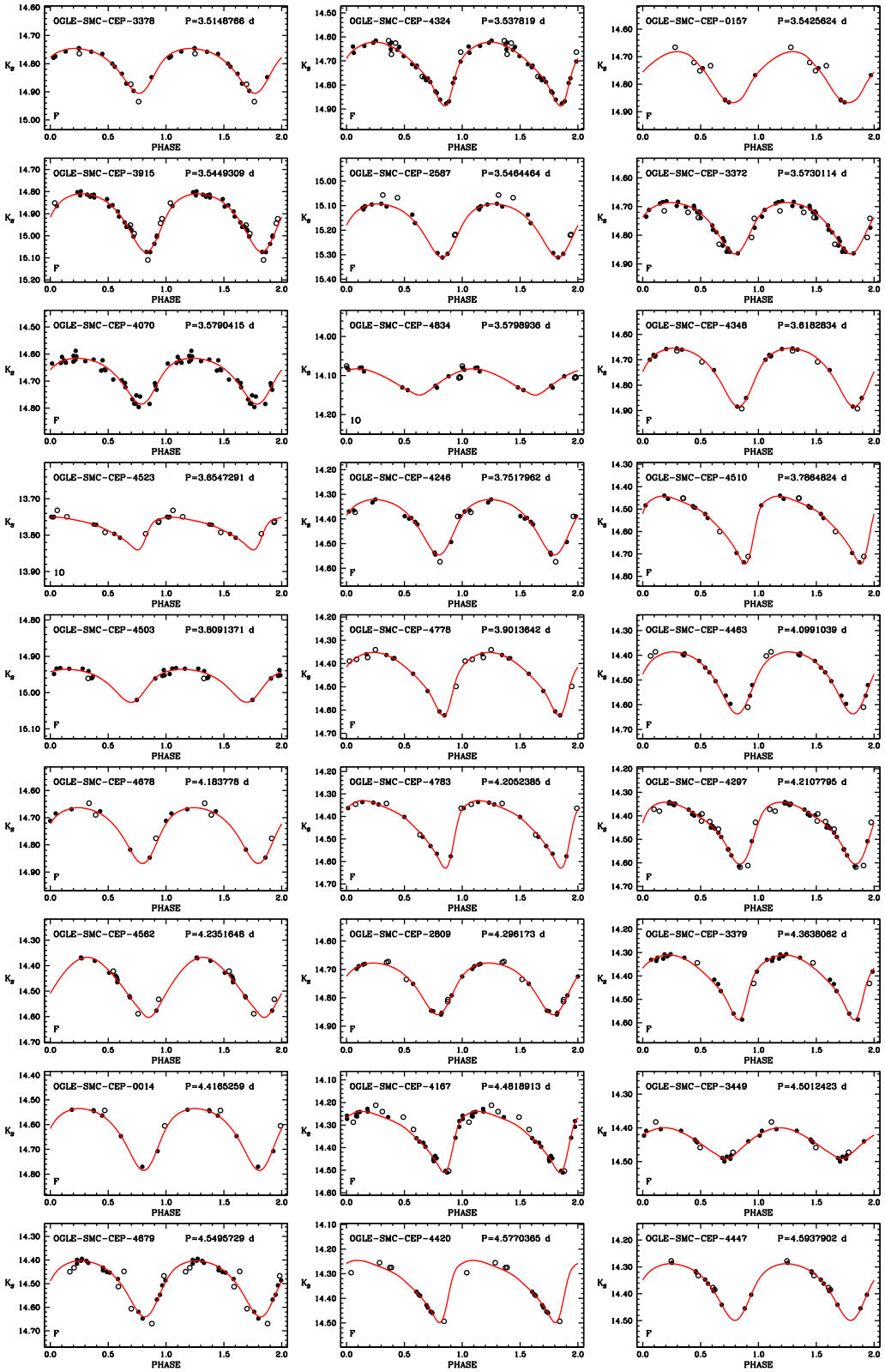

Figure A3. Same as in Fig. A1 but for the K_s.

APPENDIX B: DISTANCES OF AB-TYPE RR LYRAE STARS IN SMC AND LMC

To estimate the distances of the RR Lyrae stars in the LMC and SMC, we followed substantially the same approach of Jacyszyn-Dobrzeniecka et al. (2017). In more detail, we used (i) the V, I photometry provided by the OGLE IV survey (Soszyński et al. 2016); (ii) the theoretical $PW(V, I)$–[Fe/H] relations provided by Marconi et al. (2015) (their Table 7). The usefulness of Wesenheit magnitudes has been already discussed in this paper and we will not repeat the same considerations here. Marconi et al. (2015) calculated $PW(V, I)$–[Fe/H] relations for a variety of magnitude–colour combinations including V, I bands: $W(V, I) = I - 1.38(V - I)$. They list separately the relations for c- and ab-type RR Lyrae pulsators. However, both relations show a non-negligible dependence on [Fe/H]:

$$W(V, I) = -0.94 - 2.43 \log P + 0.15[\mathrm{Fe/H}] \quad (0.03 \text{ mag}), \quad \text{(B1)}$$

$$W(V, I) = -1.49 - 2.81 \log P + 0.13[\mathrm{Fe/H}] \quad (0.02 \text{ mag}). \quad \text{(B2)}$$

In the absence of spectroscopic [Fe/H] measurements, we can use the Fourier parameter ϕ_{31} (phase of the third harmonic minus three times the phase of the first harmonic) obtained from the Fourier decomposition of the light curve to estimate the metallicity (Jurcsik & Kovacs 1996). To this end, the ab-type RR Lyrae are more useful because they show a relation connecting P-ϕ_{31}–[Fe/H] which is better defined with respect to c-type pulsators (see e.g. Jurcsik & Kovacs 1996; Nemec et al. 2013). Therefore, we only considered ab-type RR Lyrae. They are abundant both in the LMC (25 926 objects) and SMC (4616 objects), hence statistics is not an issue. We choose to estimate the [Fe/H] value on the basis of the modern calibration of the P-ϕ_{31}–[Fe/H] relation of Nemec et al. (2013). Their work is based on high-resolution spectroscopy and high-precision photometric light curves obtained with the *Kepler* satellite (Nemec et al. 2011). To transform ϕ_{31} in the I band provided by OGLE IV into the V band, required to use the Nemec et al. (2013) P-ϕ_{31}–[Fe/H] relation (their ϕ_{31} is in the K_{p} *Kepler* photometric band, which can however be easily transformed to the V band using the conversion of Nemec et al. 2011), we adopted the following equation (Ripepi et al. in preparation):

$$\phi_{31}(V) = -(0.51 \pm 0.06) + (0.845 \pm 0.020)\phi_{31}(I) - (1.25 \pm 0.12) \log P \quad (0.12 \text{ rad}). \quad \text{(B3)}$$

We used these values to estimate the ab-type RR Lyrae metallicity using the Nemec et al. (2013) results. In turn, these [Fe/H] in conjunction with pulsator periods from OGLE IV have been inserted in equation (B1) to obtain absolute $W(V, I)$ magnitudes. A simple comparison with the observed $W(V, I)$ calculated from OGLE IV photometry, directly provided the dereddened distance modulus, and in turn the distance, for each ab-type RR Lyrae in the LMC and SMC. The derived distances have been adjusted to provide an average distance of 63.0 kpc for the SMC. We remind that the detailed structure of the SMC based on VMC observations of RR Lyrae stars is presented in Muraveva et al. (2017).

This paper has been typeset from a TEX/LATEX file prepared by the author.